

# The Intrinsic Magnetic Fields of the Galactic Black Hole Candidates

STANLEY L. ROBERTSON

*Department of Physics, Southwestern Oklahoma State University, Weatherford, OK 73096*

## ABSTRACT

Recent work has linked the quiescent luminosities and hard/soft spectral state switches of neutron stars (NSs) to their spinning magnetic fields. It is shown here that the quiescent luminosities and spectral state switches of galactic black hole candidates (BHCs) could be produced in the same way for spin rates below 100 Hz and magnetic fields above  $10^{10}$  G. It is also shown that the ultrasoft peaks and large flickering amplitudes of the BHCs would be expected from the surfaces of massive NSs. None of the few spectral characteristics that distinguish BHCs from low mass NSs have been explained in terms of event horizons. Serious consideration of the possibility that they might simply be massive NSs opens an avenue for proof of event horizons by negation, but requires the use of a space-time metric that has no event horizon. The Yilmaz exponential metric used here is shown to have an innermost marginally stable orbit with radius, binding energy and Keplerian frequency that are within a few percent of the same quantities for the Schwarzschild metric. A maximum NS mass of  $\sim 10M_{\odot}$  is found for the Yilmaz metric. The two metrics essentially differ only by the presence/absence of a surface for the BHCs, thus enabling proof or disproof of the existence of event horizons.

*Subject headings:* Accretion, Black Hole Physics, Stars: neutron, Stars: novae, X-rays: stars

## 1. Introduction

According to General Relativity, an object of nuclear density and more than  $2.8 M_{\odot}$  would be a black hole (Kalogera & Baym 1996, Friedman & Ipser 1987). Several black hole candidates (BHCs) have been found in x-ray binary systems. At this time there are ten galactic x-ray sources known to exceed the neutron star (NS) mass limit. Only two of these, Cyg X-1 and LMC X-3, are not in low mass binary systems. Perhaps twenty more candidates have been identified via spectral similarities (e.g. see Barret, McClintock & Grindlay 1996). Active galactic nuclei (AGNs) are also generally believed to exceed a Schwarzschild mass limit, however, they will be considered here only in passing in order to restrict the scope of a lengthy article. In addition, their radii are less well constrained than those of the x-ray novae. Nevertheless, it should be noted that there are strong spectral similarities between NSs, BHCs and AGNs. Campana et al. (1998a), Becker & Trümper (1998) and van der Klis (1994) have recently reviewed NS properties, while Poutanen (1998) has reviewed BHCs and AGNs.

X-ray novae display a rich mix of spectral and timing characteristics. Many of them are keyed to the luminosity level. Luminosity generally derives from accretion of mass from a companion star via an accretion disk. Flares are caused by instabilities of the flow either from the companion or through the disk. Maximum luminosities during major flares are often  $\sim 10^6 - 10^7$  times quiescent luminosities. Maximum luminosities are often near the Eddington limit ( $\sim 2 \times 10^{38}$  erg/s for a canonical  $1.4 M_{\odot}$  NS). Complex changes of luminosities in soft x-rays (0.1-4.0 keV), hard x-rays (4-20 keV) and hard tails, (20-200 keV)

occur during flares. Hard tail luminosity with an inverse power law dependence on photon energy is prominent during the initial rise of luminosity and also during the decay. In most cases this power law component weakens substantially at high overall luminosities. “Ultrasoft” radiation (White & Marshall 1984) with a general brehmsstrahlung shape and a peak near 1 - 3 kev is often, but not always, seen at high luminosities. Observations during “dips” where some sources, seen at large inclination through absorbing materials, provide some spatial resolution, show that the soft peaks arise near the center of the the disk. BHCs simultaneously show hard tails and softer, more luminous peaks more commonly than NSs. Spectral state switches occur between soft “high” luminosity states and the harder “low” states that are characterized by power law spectral features. Hard low states typically have luminosities below  $10^{36}$  erg/s for NSs and below  $10^{37}$  erg/s for BHCs. Campana et al. (1998) and Zhang, Yu & Zhang (1998) have attributed the spectral state switch to “propeller effects” (Illarionov & Sunyaev 1975) of magnetic fields for NSs. Black hole models usually attribute the switch to accretion disk instabilities. In either case, it is generally accepted that the hard spectrum of the low state originates in the accretion disk and that it persists, usually becoming harder, as quiescence is approached. There is no consensus about how it is produced. The strong similarities of quiescent NSs and BHCs (Tanaka & Shibasaki 1996) suggest that a common mechanism produces the quiescent luminosity.

Low frequency,  $\approx 6$  Hz, quasi-periodic oscillations (QPOs) often appear in suitably high states (Fortner, Lamb & Miller 1989, Miyamoto, Kimura & Kitamoto 1991, Mak-

ishima et al. 1986) of both NSs and BHCs. Large amplitude flickering ( $\approx 10^{-3}$  - 10 s luminosity variation) occurs when power law components are dominant, particularly at intermediate luminosity (Balucinska-Church et al. 1997, Tennant, Fabian & Shafer 1986, Stella et al. 1985). The variations of hard and soft x-rays are often correlated (usually with delayed hard photons) on short time scales ( $< 1$  s), but are uncorrelated (Pan et al. 1995) or anti-correlated on scales of hours or more. All of these features, some of which were once thought to be black hole signatures, have been observed in both BHCs and NSs (e.g., see Singh et al. 1994, Barret, et al. 1992, Churazov, et al. 1995, Stella et al. 1985, Tanaka 1989, van der Klis 1994). Cir X-1, which was dropped from the BHC list after displaying surface thermonuclear bursts, shows most of these characteristics. Its wide array of spectral characteristics is likely due to a rather wide variation of accretion rates associated with an eccentric orbit.

Some NSs show some features that are not obviously shared by BHCs. Radio or x-ray pulsations, and surface thermonuclear bursts are NS signatures that have only been found in erstwhile BHCs such as Cir X-1. NSs usually show bursts or pulses but not both. The accepted explanation for this dichotomy is a magnetic field, a NS signature, that can concentrate accreting matter in magnetic pole regions where fusion proceeds at rates high enough to suppress bursts (Taam & Picklum 1978). Bursts are generally not observed for pulsars with  $\sim 10^{11}$  G magnetic fields, but have been observed for millisecond pulsars, which have weaker fields. Interaction of the accretion flow with the NS magnetic field is believed to account for the characteristics of color-color diagrams and hardness-intensity

diagrams of “Atoll” and “Z” type NSs. These sources have magnetic fields of  $\sim 10^8$  G and  $10^9$  G, respectively (White and Zhang 1997). The peak accretion rates of Zs are near Eddington limits, while those of Atolls are much lower. Van der Klis (1994), who developed much of the Atoll-Z phenomenology has provided a review and a discussion of the similarities between the various states of BHCs and NSs; particularly the strikingly similar time-resolved power density spectra of flickering Atolls and BHCs.

The presence of a hard spectral tail at overall luminosity levels above  $10^{37}$  erg/s is considered to be a reliable signature of a BHC (Barret, McClintock & Grindlay 1996). Why an accreting black hole should have this property is not understood (Kusunose, Minishige & Yamada 1996, S.N. Zhang, et al. 1997). With this exception, the lack of spectral or timing signatures of black holes has left mass determination as the only way to certify a BHC (McClintock 1998). Until signatures of event horizons are found, it remains feasible to suppose that the BHCs might simply be massive neutron stars. The point of this work is to explore this possibility.

BHCs as compact, massive NSs could possess magnetic fields, and should have large surface binding energies and substantial redshifts of surface radiations. Magnetic fields would permit a common mechanism for the spectral state switches of BHCs and NSs. Larger surface binding energies and redshifts for the more massive BHCs would make their surface emissions both brighter and softer. It would seem necessary to reject these possibilities before acceptance of the reality of event horizons for the BHCs. In order to pursue these possibilities in a quantitative way, a space-time metric that has no event horizon

is needed. The Yilmaz metric (YM) has been adopted here for this purpose. The massive NS hypothesis discussed here is only weakly dependent on metric properties in general, but depends crucially on the distinctions between surfaces and magnetic fields *vs* event horizons. It is shown here that YM and SM accretion disks have such similar properties that they essentially differ only by the presence/absence of a surface.

Although most of the mathematical details have been placed in an appendix, a comparison of the two metrics is given in Section 2. Results for the two metrics for a simple model of a star of constant proper density (Clapp 1973) are also given. An object of this sort with a density in its outer layers corresponding to nuclear saturation density provides a rough approximation of a neutron star with a fairly stiff equation of state. It provides very conservative estimates of the radiant energy and redshifts to be expected for accretion reaching a massive NS surface. Magnetic field phenomena that affect the accretion flow and spectral characteristic are outlined in Section 3. Section 4 discusses magnetic and strong-field gravitational effects in NSs and BHCs. Section 5 considers the origins of various spectral characteristics and the implications for massive NS models.

## 2. The Yilmaz Metric

While not widely known, the Yilmaz theory (Yilmaz 1958, 1971, 1975, 1992, 1994, 1995) has some interesting positive features that may help to resolve the hiatus between General Relativity and Quantum Mechanics. At this time, it is quite clear that one or both of these landmark theories of the twentieth century must be modified before they can be fully compatible. The Yilmaz theory modifies

General Relativity primarily by the explicit inclusion of the stress-energy of the gravitational field as a source of space-time curvature. With a true field stress-energy the Yilmaz theory possesses a field Lagrangian and can be quantized (Yilmaz 1995).

Although the Yilmaz theory has been criticized, (Will 1981) the criticism appears to be based on an incorrect assumed form of the metric (Yilmaz 1981). For the present purposes, the essential features of any alternative metric would be lack of event horizons and readily calculable NS characteristics. Nevertheless, the Yilmaz theory passes the four classic weak-field tests. It permits local energy-momentum conservation and has no adjustable parameters, no singularities and no event horizons (Alley 1995, Yilmaz 1994). Gravitationally compact objects can exist in the YM but they are not black holes. Radially directed photons can always escape.

The metric of space-time in the vicinity of neutron stars is dominated by the gravity of the star which is considered here to be a static object. The static limit interval in the Yilmaz exponential metric is:

$$ds^2 = g(r)c^2dt^2 - (dr^2 + r^2d\theta^2 + r^2\sin^2\theta d\phi^2)/g(r) \quad (1)$$

where:

$$g(r) = \exp(-2u(r)) \quad (2)$$

and  $u(r)$  is the gravitational potential. In the SM:

$$ds^2 = g(r)c^2dt^2 - dr^2/g(r) - r^2d\theta^2 - r^2\sin^2\theta d\phi^2 \quad (3)$$

and:

$$g(r) = 1 - 2u(r) \quad (4)$$

The gravitational potential at distance  $r$  from mass  $M$ ,  $u(r) = GM/c^2r$  reaches  $\sim 2 \times 10^{-6}$  at

the photosphere of the sun,  $\sim 3 \times 10^{-5}$  in the solar system relative to the Great Attractor,  $\sim 10^{-3}$  at the smallest AGN radii of which we can be certain,  $\sim 0.17$  at the innermost marginally stable orbit of a NS or BHC,  $\sim 0.25$  at the surface of a maximum mass NS in the SM and 0.5 at the event horizon of a black hole. The five orders of magnitude jump from the solar system testing ground to the neutron star regime is good reason for caution about the acceptance of any strong-field theory of gravitation.

The exponential metric can be inferred from special relativity and the principle of equivalence applied to frames co-moving with an accelerated particle (Einstein 1907, Rindler 1969, Yilmaz 1975). This is a strong indication that the exponential metric is the proper static limit for gravitation. That this metric does not satisfy the field equations of General Relativity was one of the motivations for the earliest version of the Yilmaz theory (Yilmaz 1958). It is noteworthy that the exponential metric is merely rescaled by addition of an arbitrary constant to the potential whereas the SM depends on an absolute potential. Without this dependence, event horizons could be transformed away. With the conventional choice of zero potential at infinity, however, the two metrics are the same to first order in  $u(r)$ . This is sufficient to insure that they give the same results in the four classic weak-field tests of General Relativity. Gravitational redshift of radiation observed distantly is given by (Rindler 1969):

$$z = \exp(u(r)) - 1 \quad (5)$$

and in the SM:

$$z = \frac{1}{\sqrt{1 - 2u(r)}} - 1 \quad (6)$$

### (i) Accretion Mechanics

In either metric there is an innermost marginally stable orbit that can be reached by an accreting particle. The orbital radius is (see appendix)  $r_{ms} = 4/(3 - \sqrt{5})GM/c^2$  in the YM. Thus  $u(r_{ms}) = 0.191$ . In the SM  $r_{ms} = 6GM/c^2$  and  $u(r_{ms}) = 1/6$ . An accreting particle starts from a large radial distance, with essentially zero momentum and  $u(r) \approx 0$ . Its energy is  $E = m_0c^2$ . At  $r_{ms}$  in the YM, the energy is  $E = 0.945m_0c^2$  (see appendix). The binding energy at  $r_{ms}$  is the difference,  $0.055m_0c^2$ . Whether this is radiated or advected depends on the opacity of the accretion disk and the viscous dissipation mechanisms. For any circular orbit in the disk, the particle energy in the YM can be shown to be  $E = m_0c^2 \exp(-u)\{(1 - u)/(1 - 2u)\}^{1/2}$ . Thus, in the YM the maximum fraction of accretion mass energy which can be observed as radiation from the disk is:

$$f_d = 1 - \exp(-u)\sqrt{\frac{1 - u}{1 - 2u}} \quad (7)$$

limited to  $u < 0.191$ . For the SM the maximum fraction of accretion mass energy which can be radiated from the disk, limited to  $u < 1/6$  and  $0.057m_0c^2$ , is:

$$f_d = 1 - \frac{1 - 2u}{\sqrt{1 - 3u}} \quad (8)$$

If the innermost marginally stable orbit is the inner disk boundary, disk mechanics and disk luminosity should be only weakly mass dependent and very nearly the same for the two metrics. The binding energy at  $r_{ms}$  differs by only 3.6% in the two metrics. It is independent of both the mass of the central object and  $r_{ms}$ . For the star model used here, disks would terminate at  $r_{ms}$  above the surface for NSs with masses above  $2.1 M_\odot$  (YM) or 1.7

$M_\odot$  (SM). For stars with sufficiently weak magnetic fields ( $< 10^7 G$ ) this “gap accretion” would produce a hard power-law spectrum (Kluzniak & Wilson 1991, Hanawa 1991, Walker 1992) arising from bulk flow Comptonization in a boundary layer. In fact, however, radiation (Miller, Lamb & Psaltis 1997) and/or magnetic torques (Lai 1998) on the disk appear to cause the inner disk radius of NSs to be larger yet. At present it seems likely that kHz QPOs may be generated at the sonic point just inside the disk (Miller, Lamb & Psaltis 1997). The observed QPO frequencies indicate that the sonic radius is generally larger than  $r_{ms}$ , but may approach  $r_{ms}$  as a limit at sufficiently high accretion rates (Zhang, et al. 1998).

The Keplerian frequency of the innermost marginally stable orbit is of considerable interest. In the YM, Keplerian frequencies are given by:

$$\nu_K = \frac{\sqrt{GM} \exp(-2u)}{2\pi r^{3/2} \sqrt{(1-u)}} \quad (9)$$

For the innermost marginally stable orbit,  $u = 0.191$  and  $r_{ms} = 5.24GM/c^2$ , this yields  $\nu_K = 2040M_\odot/M$  Hz, compared to 2200  $M_\odot/M$  Hz in the SM; a mere 7% difference.

For neutron stars there is additional energy dissipated as accreting particles are brought to rest on the surface. Neglecting the effects of star spin and evaluating the energy-momentum four-vector for zero momentum shows the energy of a particle at rest on a star of radius  $R$  to be  $E = m_0 c^2 \sqrt{g(R)}$ . Thus the total accretion energy, external to the star, which may be directly radiated to distant observers is  $m_0 c^2 (1 - \sqrt{g(R)})$ . The fraction radiated from the star surface itself (neglecting fusion, which can be considered as part of the

binding to the star) would be:

$$f_s = 1 - \sqrt{g(R)} - f_d \quad (10)$$

In the strong-field cases to be considered here, over half of the energy release exterior to the star occurs within  $3R$  and  $\approx 90\%$  from within  $10R$ .

### (ii) Compact Objects

A compact object of constant proper density (Clapp 1973) is considered here. The details are straightforward, but tedious, and have been placed in the appendix. The proper density is  $\rho(r)g(r) = \rho_0$ , a constant. These compact objects have a characteristic radius and mass that are given by:

$$r_0 = \frac{c}{\sqrt{4\pi G \rho_0}} \quad (11)$$

$$M_0 = \frac{c^2 r_0}{G} \quad (12)$$

As shown in Table 3,  $g(R)$  reaches 0.25 at the surface of a maximum mass NS in the SM. Assuming that  $\rho(R) = 2.7 \times 10^{14} \text{ g/cm}^3$ , the nuclear saturation density, and using  $g(R) = 1 - 2u(R)$  yields  $\rho_0 = 1.35 \times 10^{14} \text{ g/cm}^3$ . This value of  $\rho_0$  yields:  $r_0 = 28.2 \text{ km}$  and  $M_0 = 19M_\odot$ . In turn, these yield a maximum mass of  $2.45M_\odot$  for 14.3 km radius and a maximum radius of 15.5 km for the SM. Independent of the choice of  $\rho_0$ , NSs in the upper one third of the mass range permitted by the SM would have  $u(R) > 1/6$  and have radii small enough for gap accretion.

For the same  $\rho_0$  in YM, the maximum mass is  $9 M_\odot$  at a radius of 13.5 km. A maximum radius of 18.8 km occurs for about  $5.1 M_\odot$ . Mass vs. radius curves are similar in shape to those obtained by Friedman & Ipser (1987) for their core model. Although the constant

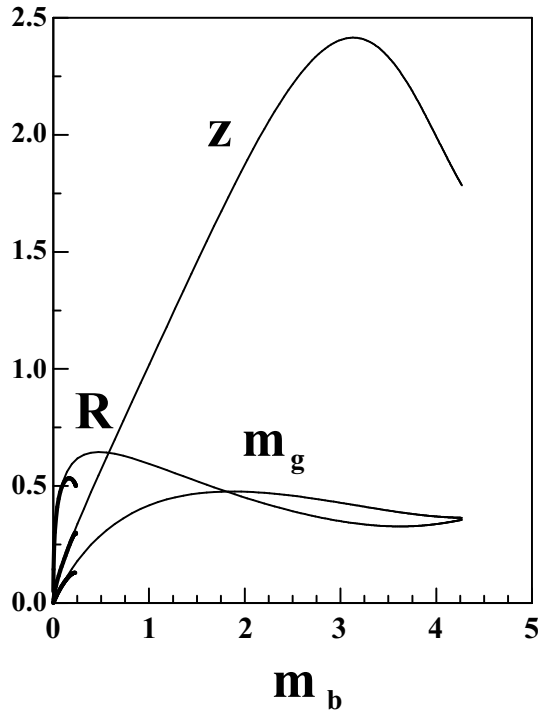


Fig. 1.— Radius,  $R$ , gravitational mass,  $m_g$ , and surface redshift,  $z$ , as functions of free baryon mass,  $m_b$ , contained within a neutron star in the exponential metric. Radius is in units of  $r_0 = c/\sqrt{4\pi G\rho_0}$  and masses in units of  $M_0 = c^2 r_0/G$ . Heavy line features at the lower left are the same quantities for the SM.

proper density model fails to properly account for the softer exterior layers for low mass objects, this will be of no concern here. The effects of stellar rotation may increase maximum masses (Friedman & Ipser 1987) by about 25%, to about  $3 M_\odot$  for the SM and  $11 M_\odot$  for the YM. Figure 1 shows comparisons of mass, radius and surface redshift for YM and SM. It is interesting that there exists a maximum mass for the YM that is dependent on density. For nuclear density, an  $11 M_\odot$  maximum mass may be adequate to cover the range of masses that have been found for the galactic BHCs. Figure 2 shows properties for the SM in more detail.

Tables 2 and 3 give masses, radii, surface potentials, surface redshifts, etc for the two metrics. With these quantities, the necessary binding fractions of the disk and surface can be calculated using equations 7 - 9. Figure 3 shows these binding fractions. A profound effect of a neutron star surface is implied by Fig 3. Up to about  $\approx 1.4 M_\odot$ , the luminosity would be fairly evenly divided between disk and surface, but for the largest masses in the Schwarzschild metric up to 80% of the luminosity might arise inside the last stable orbit; near or on the star surface. In the YM as much as 90% of the luminosity could originate from the star surface. The binding fractions at the star surface can reach 70% for large masses in the YM. Large binding fractions and redshifts would make their surface radiations very prominent and very soft.

### (iii) Internal Processes

After accreted matter reaches the surface there is still energy to be produced by fusion and a need for additional gravitational binding energy to be released for stability of the star. In order to properly account for all of the energy available, one needs to consider the dif-

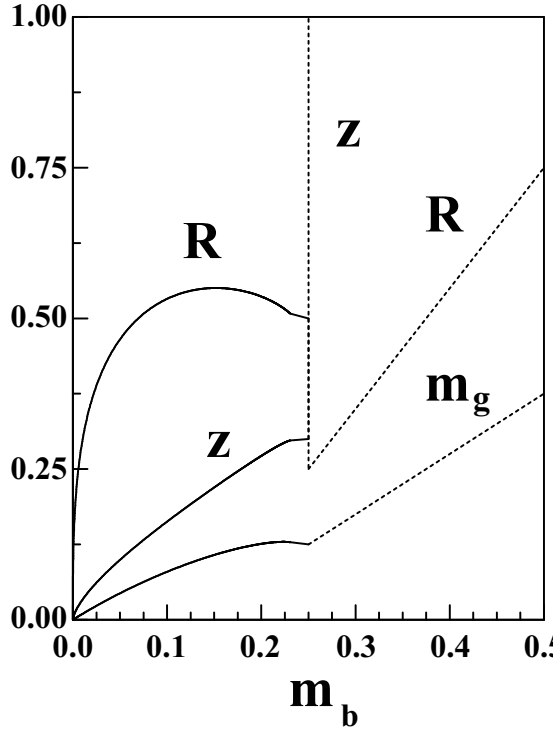


Fig. 2.— Radius, gravitational mass and surface redshift as functions of free baryon mass for a neutron star in the Schwarzschild metric. Units are the same as Figure 1. Dashed lines show extensions for black holes.

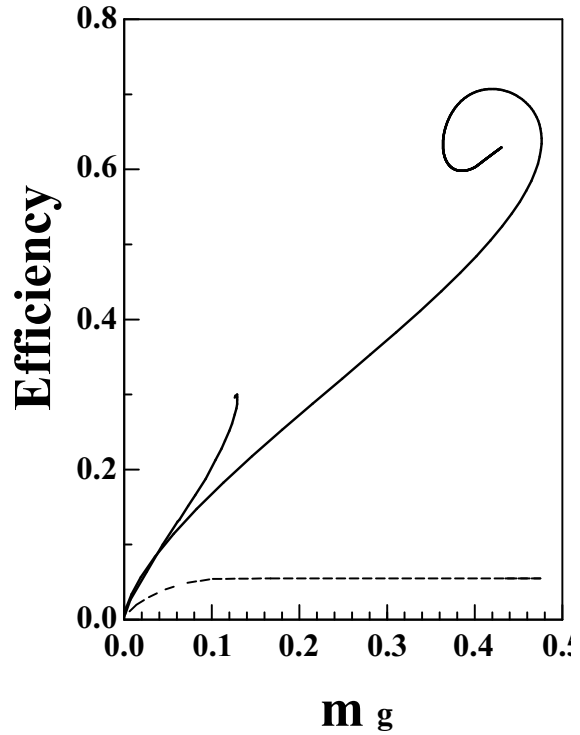


Fig. 3.— Efficiencies of conversion of gravitational potential energy to radiation as functions of gravitational mass,  $m_g$ . Gravitational mass is in units of  $M_0$ . Solid upper lines are  $(f_s + f_d)$ . Free baryon mass,  $m_b$ , increases from left to right along these curves. The spiral of the YM occurs because maxima and minima of redshift and gravitational mass do not correspond to the same free baryon mass. Lower dotted line is  $f_d$ , which is essentially the same in both metrics. Surface radiation is represented by the difference between the upper and lower lines, excepting black holes.

ference between free baryon mass and mass bound gravitationally within the star. The total gravitational energy release as rest mass  $\Delta m_b$  falls from a large distance and becomes bound in the star would be  $c^2(\Delta m_b - \Delta m_g)$ , or  $c^2\Delta m_b(1 - dm_g/dm_b)$ . The term in parentheses being the maximum possible fraction of accreted rest mass to be converted to radiations seen by a distant observer. It is plotted in Figure 4 as the gravitational binding fraction of the object. For a neutron star in the SM, it actually diverges shortly after it reaches 1.0 just below  $2.35 M_\odot$ . At this point the constant intrinsic density model fails in the SM. The addition of more mass simply causes a core collapse, though it may be possible that some of the binding energy would escape through neutrino emission, pair production and gravitational radiation.

In the YM there is no discontinuity of binding fraction but after trapped baryons produce a maximum gravitational mass, the star can become more tightly bound. The more massive neutron stars permitted in either metric swallow baryons but must radiate their mass equivalents for stability. It is apparent that the overall binding fraction is much larger than the binding fraction at the surface. Some substantial additional radiations of internal origin should be seen from accreting NSs in either metric. It is possible that this energy would appear as copious photon, pair production or neutrino emissions, or gravitational radiation. Pair plasma emissions might be part of the jets observed for some NSs and BHCs (Gliozzi, Bodo, & Ghisellini 1998). Whether or not accretion energy might be transiently stored has not been considered here, but it should be noted that mass-energy can be trapped inside the photon sphere for  $u(R) > 1/2$  (YM) or  $1/3$

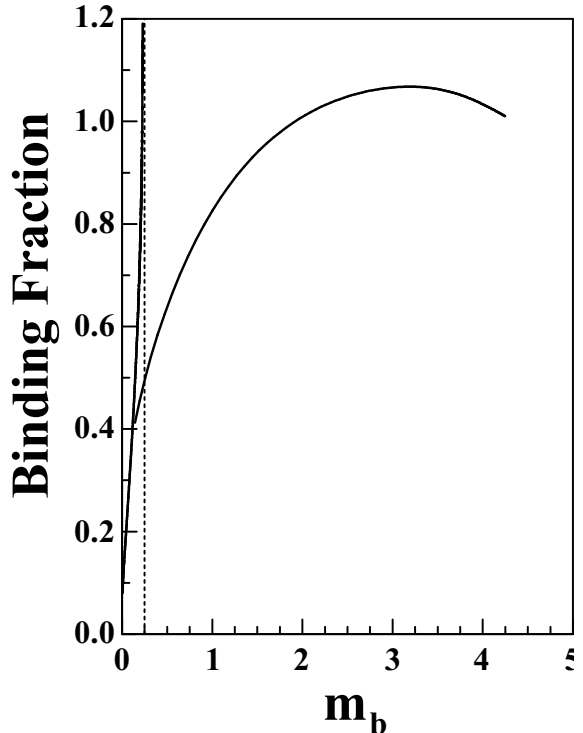


Fig. 4.— Binding energy expressed as a fraction of the rest mass-energy of accreted particles; given by  $(1 - \frac{dm_g}{dm_b})$ . Collapse of the core in the Schwarzschild metric is shown by the diverging line at the left. The curved line extending to the right is for the Yilmaz metric.

(SM). Spectral qualities of surface radiations should also be affected when the surface lies inside the photon sphere, however, this would involve analysis well beyond the scope appropriate for this work.

### 3. Magnetic Phenomena

The magnetosphere radius can be estimated as the radius for which the impact pressure of accreting matter is some fraction,  $\eta$ , of magnetic pressure (e.g., Lamb, Pethick & Pines 1973). For dipole fields and disk accretion, with Keplerian motion outside the magnetopause, this criterion yields :

$$r_m = \left( \frac{\eta^2 \xi^2 B^4 R^{12}}{2\epsilon^2 G M \dot{m}^2} \right)^{\frac{1}{7}} \quad (13)$$

where  $\epsilon$  is the ratio of radial flow velocity to free fall velocity in a spherical flow,  $2\xi$  is the ratio of disk thickness to radius and  $B$  is the magnetic field at  $R$ . A choice of  $(\eta\xi/\epsilon)^{2/7} = 0.35$  brings the magnetospheric radius into close agreement with that of the much more complicated model of Ghosh & Lamb (1992). Using  $\eta\xi/\epsilon = 0.025$ ,  $M = 2.8 \times 10^{33} M_{1.4} g$ ,  $B = 10^9 B_9 G$ ,  $R = 10^6 R_6$  cm and  $\dot{m} = 10^{15} \dot{m}_{15}$  g/s this becomes:

$$r_m = (78 km) \left( \frac{B_9^4 R_6^{12}}{M_{1.4} \dot{m}_{15}^2} \right)^{\frac{1}{7}} \quad (14)$$

The magnetosphere radius shrinks to accommodate higher impact pressure. It is relatively impermeable to diamagnetic plasma, but unstable for curvature perturbations (Rayleigh-Taylor). Arons et al. (1984) have described shot penetrations of the magnetopause and their further fragmentation via Kelvin-Helmholtz processes as they fall through the co-rotating magnetosphere. At relatively low accretion rates individual shots may produce considerable flickering. The larger surface binding

fractions for more massive objects in the YM might explain the larger amplitude flickering observed for BHCs. For recent reviews of magnetospheric phenomena, see Campana et al. (1998a) and Becker and Trümper (1997). It is well-known that pulsars can generate very hard spectra via magnetospheric effects (Michel 1991, Becker & Trümper 1997) and surface impact (Alme & Wilson 1973) as well as in shock fronts where magnetospherically expelled matter impinges on nebulae.

The star spin frequency determines the co-rotation radius,  $r_c$ , for which the magnetospheric equator rotates at the Keplerian orbit frequency. In (SM),  $r_c = (GM/4\pi^2\nu_S^2)^{1/3}$ . When the magnetospheric radius lies outside the co-rotation radius, accreting matter receives a super-Keplerian push at the magnetopause. It is swept outward and is unable to penetrate the magnetosphere until a boundary layer with sufficient pressure builds. This is the well-known “propeller effect” (Illarionov & Sunyaev 1975). When the magnetosphere is forced inside the co-rotation radius, the spectrum changes from a hard, low state to a state of higher luminosity and softer spectrum due to greater surface contributions. If the transition radius is large there may be a large flare as mass strikes the star. Since the co-rotation radius is determined by the spin, there is a strong luminosity-spin correlation for these flares (Stella, White & Rosner 1986). Additional evidence has recently been found (Cui 1997) for propeller effects in the accreting x-ray pulsars, GX 1+4 and GRO J1744-28. Sharp transitions were observed at luminosities of  $\sim 10^{37}$  erg/s, for which x-ray pulsations ceased, but became re-established at slightly higher luminosity levels. Zhang, Yu & Zhang (1998) and Campana, et al. (Campana, S. et al. 1998b) have indepen-

dently analyzed the decline of the 1997 outburst of Aql X-1 and found strong evidence of a propeller effect and an accompanying spectral state transition with very little luminosity change. The transition was followed by a rapid cutoff of luminosity that was arrested only briefly as radiation pressure from the surface emissions ceased.

For sufficiently large  $r_c$ , the maximum luminosity that can be achieved without surface contributions corresponds to  $r_m \approx r_c$  and  $L_c = GM\dot{m}/2r_c$ :

$$L_c = \frac{2\sqrt{2}\eta\xi\pi^3B^2R^6\nu_S^3}{\epsilon GM} \quad (15)$$

or

$$L_c = (1.2 \times 10^{34} \text{ erg/s}) B_9^2 R_6^6 \nu_2^3 M_{1.4}^{-1} \quad (16)$$

where  $\nu_S = 100\nu_2$  Hz. Campana et al. (1998) have produced the same equation for spherical accretion except for a multiplier of 20 in place of the 1.2 used here. The smaller multiplier merely reflects the smaller magnetospheric area impacted by a disk.

For objects more massive than  $\sim 1M_\odot$ , classical physics expressions for surface luminosity are inadequate, however, we can use  $L = (yf_s + f_d)\dot{m}c^2$ , where  $y$  is the fraction of mass reaching the magnetopause that penetrates to the surface. Using this to evaluate  $\dot{m}$  and setting  $r_m \approx r_c$  in Eq. 13 provides a relation of the luminosity for accretion at the co-rotation radius to the magnetic field and spin of the star:

$$L = \frac{(2\pi)^{\frac{7}{3}}(yf_s + f_d)c^2\xi\eta B^2R^6\nu_S^{\frac{7}{3}}}{\sqrt{2}\epsilon(GM)^{\frac{5}{3}}} \quad (17)$$

or

$$L = (9 \times 10^{35} \text{ erg/s})(yf_s + f_d)B_9^2 R_6^6 \nu_2^{\frac{7}{3}} M_{1.4}^{-\frac{5}{3}} \quad (18)$$

Eqs. 16 and 18 should yield identical results for  $y = 0$ , however, since the classical and relativistic binding energies differ slightly for the inner disk, there can be spurious small differences.

$L_{min}$  will be used to designate the accretion rate for which  $y=1$ ,  $r = r_c$ , and all of the accreting matter reaches the star. If the co-rotation radius is relatively large compared to the star radius, large luminosity changes can occur at the transition from  $L_c$  to  $L_{min}$ , even if the accretion rate changes very little. Even slight departures from  $y = 0$  might produce such strong radiation pressure that the full transition to  $L_{min}$  is prevented.

The magnetosphere is limited by the light cylinder radius,  $r_{lc}$ , at which a co-rotating magnetosphere equator would move at the speed of light. For fast spinners with  $\nu_S \sim 400 \text{ Hz}$ ,  $r_{lc}$  can be less than  $\sim 120 \text{ km}$ . When the magnetospheric radius lies beyond  $r_{lc}$  the radio pulsar mechanism may become active. Both pulsed point source x-ray emissions and diffuse harder radiation at lower luminosity from a synchrotron nebula have been observed for the isolated  $\gamma$ -ray pulsar PSR 1055-52 (Shibata et al. 1997 ApJ 483, 843).

The maximum quiescent luminosity that can be produced solely by disk accretion corresponds to  $r_m = r_{lc}$ . With  $L = GM\dot{m}/2r$ , this yields:

$$L_{q,max} = \frac{\xi\eta(2\pi\nu_S)^{\frac{9}{2}}\sqrt{GM}B^2R^6}{2\sqrt{2}\epsilon c^2} \quad (19)$$

or

$$L_{q,max} = (3.4 \times 10^{30} \text{ erg/s}) M_{1.4}^{\frac{1}{2}} B_9^2 R_6^6 \nu_2^{\frac{9}{2}} \quad (20)$$

If a pulsar wind drives the quiescent luminosity, the rotational energy loss rate is (Bhat-

tacharya & Srinivasan 1995):

$$\dot{E} = 4\pi^2 I \nu_S \dot{\nu}_S = \frac{32\pi^4 B^2 R^6 \nu_S^4}{3c^3} \quad (21)$$

where  $I$  is the moment of inertia of the star. The right member of this equation is empirical, lacking magnetic axis inclination dependence and perhaps factors of  $\eta$  and  $\epsilon$ , however, it and the middle member have been taken as an operational definition of the magnetic moment,  $BR^3$ , for NSs with  $I = 10^{45} g - cm^2$ . Becker and Trümper (1997) have provided a tight correlation between x-ray luminosity and rotational energy loss rate for which the x-ray luminosity is  $1.0 \times 10^{-3} 4\pi^2 I \nu_S \dot{\nu}_S$  again with fixed  $I = 10^{45} g \text{ cm}^2$ . While most of the correlated sample likely consists of stars near  $1.4M_\odot$ , what has really been correlated is x-ray luminosity and  $\nu_S \dot{\nu}_S$ . Had a different value of  $I$  been used in the calculation of  $\dot{E}$ , the multiplier that would correlate with the x-ray luminosity would be  $1.0 \times 10^{-3} \times 10^{45}/I$ . For use with the YM,  $I = 2.85 \times 10^{45} g - cm^2$ , appropriate for  $1.4M_\odot$  and  $R_6 = 1.5$  will be used here. In this way the YM model can be satisfied while maintaining relatively accurate x-ray luminosities. Combining this with the right member of Eq. 21 yields:

$$L_q = (1.3 \times 10^{30} \text{ erg/s}) B_9^2 R_6^6 \nu_2^4 \quad (22)$$

In contrast to previous equations, this is merely a well grounded empiricism that represents some loosely defined x-ray luminosity rather than a bolometric luminosity. Still it is to be preferred over  $L_{q,max}$  for quiescent luminosity.

For accretion to reach the star surface, with quiescent luminosities of  $10^{31} - 10^{33}$  erg/s being above  $L_c$ , would require a combination of very weak field and small co-rotation radius (fast spin). If most NSs reach a spin equilibrium for long time average luminosities near those in accord with Eq. 18 with  $y$

$= 1$ , (White & Zhang 1997) then their quiescent luminosities are highly unlikely to derive from either surface accretion or accretion at the light cylinder radius.

Becker and Trümper's (1997) strong correlation of x-ray luminosity with magnetic field strength and spin rate down to luminosities well below  $10^{30}$  erg/s strongly suggests that a preponderance of the quiescent luminosity is magnetospheric. There are reasons for believing that the power-law portions of quiescent emissions originate near the magnetopause (see below). Nevertheless, some quiescent luminosity may derive from a cooling NS surface. Excess soft radiation corresponding to  $kT_{bb} \approx 0.1 - 0.2$  keV and corresponding to small  $\sim 10 - 100 \text{ km}^2$  areas has been found to be a part of the quiescent emissions of both NSs and BHCs (Tanaka & Shibasaki 1996). It is conceivable that these could be polar cap emissions of NSs, but Heindl & Smith (1998) have shown that proper attention to fluorescence and reflection substantially reduces the apparent temperature of the excess soft emissions. Further, even the remaining apparent temperature may be larger than the surface temperature of a NS, depending on its atmosphere. As shown in dips, some of the soft excess also appears to originate from an extended disk as well. Thus the origins and magnitudes of contributions to the quiescent luminosity are somewhat unclear at the present time. For this work, for luminosities generally above  $10^{32}$  erg/s, it will be assumed that the power-law magnetospheric emissions dominate the hard states. Ultrasoft blackbody ( $kT_{bb} = 0.048$  keV) surface radiation has been observed for the isolated gamma-ray pulsar, Geminga (Halpern & Wang 1997). No evidence of polar cap heating was found. Non-thermal power-law mag-

netospheric emissions in the spectral range 0.5 to 2 keV were present. Obviously, ultrasoft and power-law spectral components are not signatures of black holes. Geminga is a high energy gamma-ray source with a  $1.6 \times 10^{12} G$  magnetic field. It is the only known radio-quiet, rotation-powered pulsar with a strong magnetic field, however, some of the BHCs might also have strong fields; see below.

Brown, Bildsten & Rutledge (1998) have found that crustal heating during accretion episodes resets the core and surface temperatures of NSs and might allow them to produce quiescent luminosities of as much as  $\sim 10^{32-33}$  erg/s. An actual temperature of as little as  $\sim 0.03$  keV, would contribute  $\sim 10^{31}$  erg/s to the quiescent luminosity. This would produce a radiant equilibrium temperature of about 5000 K for optically thick matter at a distance of about  $10^5$  km. The inner accretion disk would need to be beyond this for thermal-viscous stability. For spins in excess of 0.005 Hz, the light cylinder radius is smaller than  $10^5$  km. This effectively eliminates  $L_{q,max}$  for the production of quiescent luminosity. It also sets a minimum inner radius at the start of outbursts. The inner disk must fill on a viscous timescale, producing a delay of days between the onset of optical and x-ray luminosities. Thus the 6 day delay (Orosz, et al. 1997) between the onset of optical and x-ray luminosity increases for the 1996 outburst of GRO J1655-40 would be expected. Hameury, et al (1997) have calculated 6 days as the interval for viscous inflow from  $2 \times 10^5$  km. Delays for refill of the disk have been observed for dwarf novae and for the NS, 4U 1608-52.

#### 4. The Magnetic Fields of NSs and BHCs

As additional information is acquired, some of the tentative conclusions drawn here will surely need alteration. The examples chosen are those for which I have sufficient information to initiate a discussion. They do not all fit neatly into any current scheme.

##### (i) Neutron Stars

It is well established that radio pulsars may have magnetic fields ranging from  $10^8$  G for millisecond pulsars to  $10^{13}$  G for slower spins. If not for spins revealed by bursts or kHz QPO frequency differences, it would be difficult to determine the magnetic fields of Atolls and Zs. They are not pulsars in any normal sense. Nevertheless, ratios of luminosities can be used to determine their spins and magnetic moments. Since all of the luminosity equations considered here depend on the dipole moment,  $BR^3$ , it can be eliminated by the use of luminosity ratios, thus permitting the spin to be estimated. Once the spin is known, B can be calculated. For consistency with the constant proper density star model,  $R = 15$  km for a  $1.4 M_\odot$  will be used here. Since the quantities being determined from luminosity ratios are actually spins and dipole moments, an overestimate of R may cause an underestimate of B without other effect. In order to use the ratio method, two of  $L_{min}$ ,  $L_c$ ,  $L_{q,max}$  or  $L_q$  must be identified.

*Aql X-1* is an important test case for the use of ratio methods. Campana et al (1998b, Fig. 1) reported spectral hardening beginning at  $L_{min} = 1.2 \times 10^{36}$  erg/s and complete cessation of the rapid decline at about  $1.2 \times 10^{33}$  erg/s. Identifying these as  $L_{min}$  and  $L_{q,max}$ , the ratio yields  $\nu_S = 512$  Hz for  $m_{1.4} = 1$ . This agrees moderately well with a spin

frequency of 549 Hz observed during burst QPOs. Using the QPO spin frequency and Eq. 18, a magnetic field of  $1.3 \times 10^8$  G can be calculated. Aql X-1 displays ultrasoft and power-law components in its quiescent spectrum with the power-law component accounting for more than half the luminosity. Using 549 Hz and  $1.3 \times 10^8$  G, the magnetospheric component of quiescent luminosity is calculated to be  $2.3 \times 10^{32}$  erg/s. Garcia, McClintock & Narayan (1997) report a quiescent luminosity of  $4 \times 10^{32}$  erg/s. Further, using 549 Hz and  $1.3 \times 10^8$  G permits the calculation of  $L_c = 3.8 \times 10^{35}$  erg/s, as obtained by Campana et al (1998).

*SAX J1808.4-3658* A second test case is provided by the recent outburst of the 401 Hz x-ray pulsar and burst source, SAX J1808.4-3658, (Gilfanov et al. 1998, Heindl & Smith 1998) which displayed a light curve very similar to Aql X-1. It reached a luminosity level of  $5 \times 10^{36}$  erg/s, declined slowly to about  $1.5 \times 10^{36}$  erg/s and then declined rapidly with a brief arrest at  $4 \times 10^{35}$  erg/s before reaching about  $10^{33}$  erg/s. Between the start of rapid decline and the brief arrest, 401 Hz pulsations changed from 4% rms to undetectable, thus indicating that surface impacts ceased. Identifying the luminosities at the start of rapid decline and brief arrest as  $L_{min}$  and  $L_c$  allows the calculation of a magnetic field strength of  $2.1 \times 10^8$  G, a convincing spin frequency of 419 Hz,  $L_{q,max} = 8 \times 10^{32}$  erg/s, and  $L_q = 1.7 \times 10^{32}$  erg/s.

When the accretion rate is declining, the onset of the propeller effect may be followed by a rapid cutoff of luminosity. Although many NSs (and BHCs) have shown a steep decline of luminosity from the vicinity of  $10^{36}$  erg/s, this may not always be clear evidence of the onset of a propeller effect. Without

the cessation of pulses it would have been unconvincing to identify the propeller effect for SAX J1808.4-3658. Observations of Type I bursts at luminosities above  $10^{36}$  erg/s show that accreting mass reached the surface. Yet the spectrum remained a hard power-law extending to 100 keV over two decades of luminosity change. A detailed spectral analysis (Heindl & Smith 1998) revealed the presence of iron fluorescence and a small, not very well constrained, soft excess which was modeled as a MBB. An additional unusual feature of this source is the soft x-ray lags reported by Cui, Morgan and Titarchuk (1998). An obvious possibility for explaining the unusual spectral and timing characteristics would be a very small inclination view with strong polar axial magnetospheric emissions obscuring the surface. Alternatively, there might be some unusual surface mechanism that produced the hard spectrum. At any rate, the presence of only hard spectral components cannot be interpreted as a lack of surface accretion.

The spin frequencies determined from luminosity measurements for Aql X-1 and SAX J1808.4-3658 are in convincing agreement with burst QPO frequencies, however, if their assumed masses had been doubled, their calculated spins would have been halved and their magnetic fields roughly doubled. For 4U 1636-54 and KS 1731-26, the frequency difference of kHz QPOs has been near half of the burst QPO frequency (Swank 1998). The question arises as to what is the true spin frequency. In this case it seems to be the burst QPO frequency. It has been suggested that the burst QPO frequency might be double the actual spin frequency due to two antipodal hot spots on the star. It seems improbable that bursts would be simultaneously initiated at two different places on the

star surface (Strohmayer et al. 1998). On the other hand, the detonation of some  $10^{18}$  megatons at one pole might quickly ignite another pole less than 50 km distant, depending on the shielding afforded by an intervening stellar mass (Miller 1998).

*4U1608-52* provides another test case for the use of ratios. Spectral hardening began in decline at  $L_{min} = 10^{37}$  erg/s (Mitsuda et al. 1989). Garcia, McClintock & Narayan have reported a quiescent luminosity of  $L_q = 2x10^{33}$  erg/s, while Tanaka & Shibasaki (1996) report  $6x10^{32}$  erg/s. For these luminosities, the ratios  $L_{min}/L_q$  and Eqs. 18 and 22 yield spins of 566 Hz and 275 Hz. The frequency difference of twin kHz QPOs for this source is near 230 Hz, however, this might be only half of a 460 Hz actual spin frequency. The conflicting luminosity data leave this case unresolved, but it illustrates an important point; that the results are probably correct to within small numerical factors anyway. The magnetic fields estimated from  $L_{min}$  and the two QPO spins are  $4.6x10^8$  G and  $8.4x10^8$  G. The higher spin and weaker field are the more likely attributes of an Atoll source.

*4U 1820-30* apparently has a mass in excess of  $2 M_{\odot}$  based on its kHz QPO limit frequency of 1060 Hz (Zhang, et al. 1998). Based on QPO frequency differences it spins at either 275 or 550 Hz. Both of the high frequency QPOs were visible in the low state at a luminosity of  $1.5x10^{37}$  erg/s but cut off when the spectrum softened for luminosities in excess of  $3.1x10^{37}$  erg/s. Assuming that the start of twin QPOs would correspond to mass reaching the surface implies  $L_{min} = 1.5x10^{37}$ . For  $2 M_{\odot}$ , Eq 18 yields either  $5x10^8$  G or  $1.1x10^9$  G. The higher field would be an unusually strong field for an

Atoll source, but perhaps not for one of  $2 M_{\odot}$ . Calculated quiescent luminosities for the two cases are  $5x10^{33}$  erg/s and  $1.5x10^{33}$  erg/s. Spin and magnetic field estimates for other Atoll sources, *4U 2129 + 47*, *KS 1731-26* and *4U 1730 - 335* are included in Table 1.

*Cir X-1*: Neither spin rate nor mass are available for the enigmatic *Cir X-1*.  $L_{min} = 6.3x10^{38}$  erg/s and  $L_c = 3x10^{37}$  erg/s can be determined from observations just before and two hours after a spectral hardening transition on Sept 20-21, 1977 (Dower, Bradt & E Morgan 1982). The ratio permits an estimate of a 32 Hz spin followed by a magnetic field estimate of  $8x10^{10}$  G. These results were obtained for  $M_{1.4} = 1.0$  and  $R_6 = 1.5$ . If the mass of *Cir X-1* were  $7M_{\odot}$ , the spin would be 38 Hz and the magnetic field  $8.2x10^{10}$  G. The luminosity ratio method is relatively insensitive to mass, provided that the correct accretion efficiency is used. The calculated quiescent luminosity from Eq. 22 is  $(0.9 - 6)x10^{33}$  erg/s, which is well below detector sensitivities. *Cir X-1* experiences a much wider range of accretion rates on orbital time scales than most NSs. Bradt, Shirey and Levine (1998) have provided a fascinating series of hardness-intensity diagrams for this source.

The Z and Atoll NSs of Table 1 have relatively small differences between  $L_{min}$  and  $L_c$  due to their rapid spins. The ratio of these,  $\Delta$ , should be:

$$\Delta = \frac{yf_s + f_d}{f_d} \quad (23)$$

To first order with  $y = 1$ ,  $r = r_{ms}$  in the numerator and  $r = r_c$  in the denominator,  $\Delta \approx 2u(R)/u(r_c) \approx 2r_c/R \approx 2 \sim 3$  for fast spins. This result has been discussed for spherical accretion by Corbett (1996). The bolometric luminosity change when the mag-

netopause reaches the co-rotation radius may be much smaller than implied by the ratio  $2r_c/R$  if  $y < 1$ .

If NSs of the fast spin Atoll and Z classes have been spun up to high equilibrium spin rates by accretion, then the long-term average luminosity would be near  $L_{min}$ . White and Zhang (1997) used these luminosities and the known spins of several Atoll and Z class NSs to estimate their magnetic fields. Values of  $L_{min}$  or  $L_c$  found for the spectral state transitions of several other NSs have been used here to determine some of the NS magnetic fields shown in Table 1. The results, though intentionally sparse, fit the pattern suggested by van der Klis (1994) and found by White and Zhang (1997). Z sources appear to have fields that are stronger than those of Atolls. There appears to be a  $L_{min} \propto B^2$  correlation in the results. White and Zhang suggested that the correlation might be spurious; that there might be comparable magnetic fields in all cases with a magnetospheric radius that is more weakly dependent on accretion rate for Zs where radiation pressure dominates the inner disk. The clear differences of properties of Atolls, Zs and Cir X-1 suggests that the correlation represents a progression of a real physical property.

Kilohertz QPOs have now been observed for many NSs, including both Atoll and Z types. The Atoll source 4U 1820-30 showed a limit frequency of 1060 Hz, which appears to correspond to the innermost marginally stable orbit for  $\sim 2M_\odot$  (Zhang, et al. 1998). This mass estimate obtained from the limit frequency of the QPO must be taken seriously. Cyg X-2, a Z source with a mass  $> 1.9M_\odot$  found from orbit parameters (Casares, Charles & Kuulkers 1998) has produced kHz QPOs of 1007 Hz but without reaching a lim-

iting frequency; perhaps implying a mass near  $2M_\odot$ . The BHC GRO J1655-40, at  $7 M_\odot$  (Bailyn et al. 1995) has produced a 298 Hz QPO while in a high luminosity state (Remillard et al 1997). If this is the Keplerian frequency of the marginally stable orbit it implies a mass of  $7.4 M_\odot$  (SM) or  $6.8 M_\odot$  (YM). One clear implication of these results is that the accretion disks of both NSs and BHCs may reach the innermost marginally stable orbit. With binding fractions limited to about 6% in all such cases, the differences between NSs and black holes must be found inside the last stable orbit, in the differences between surfaces and event horizons. The disks, excepting differences due to irradiation from the central source, should be much the same, (excepting those of Kerr metric black holes).

If kHz QPOs arise from clumps of mass falling from the inner disk radius to the surface, then the disk inner radius must be less than the co-rotation radius. Radii of Keplerian orbits at the frequencies at which kHz QPOs first appear are generally about two thirds of the magnetospheric radii determined from Eq. 13. Dong Lai (1998) has suggested that the sonic radius might be identical with the magnetosphere radius when outside the innermost marginally stable orbit. This might be accommodated here by suitable choice of the impact pressure-magnetic pressure balance. To do so would reduce the magnetosphere radii calculated from Eq. 14 and change the calculated dipole moments determined from the luminosity equations without other effect.

## (ii) Black Hole Candidates

If BHCs are really massive NSs that show neither pulses nor bursts then spectral state switches and ratio methods must be used to determine their spins and magnetic fields. As

is the case for Atolls and Zs, coincident spin and magnetic axes are necessary to account for the absence of x-ray and radio pulses. For BHCs, it is possible in some cases to treat the inner disk radius determined from MBB fits to spectra as a co-rotation radius. If the massive NS hypothesis is correct, then the substantial surface contributions may explain the small inner radii that are often found for MBB fits to BHC high state spectra. For low states, however, in which surface accretion is largely blocked by propeller effects, the BHC spectral models are quite applicable to NSs. Table 1 lists estimated spin and magnetic field parameters for the BHCs discussed below.

*GRS 1124-68* shows characteristics that clearly illustrate the nature of the spectral state switch. Misra & Melia (1997) showed that its inner disk radius increased to about  $27R_g$  ( $R_g = 2GM/c^2$ , 400 km for  $5 M_\odot$ ) after the spectral state transition. Ebisawa, et al (1994) give a luminosity of  $L_c = 6.6 \times 10^{36}$  erg/s for the low state. The assumption of  $r_c = 400$  km permits estimates of  $\nu_S = 15$  Hz and  $B = 1.1 \times 10^{11}$  G. In turn  $L_{min} = 2.4 \times 10^{38}$  erg/s. Eq 22 yields  $L_q = 3.9 \times 10^{32}$  erg/s. The calculated  $L_{min}$  fortuitously agrees exactly with observations. The observational upper limit for quiescent luminosity is  $4 \times 10^{32}$  erg/s, which is consistent with  $L_q$  calculated for the pulsar wind mechanism.

Życki, Done and Smith (1998) fitted the spectrum of GRS 1124-68 with a power-law plus a reprocessed fraction that included an iron line, and a relatively cool disk extending from  $r_{in}$  to  $5 \times 10^4 R_g$  (with  $R_g$  as defined above). A soft thermal component was modeled separately by optically thick Comptonization of soft seed photons from a MBB. By separately accounting for soft components their model would not have  $r_{in}$  forced to a

small value corresponding to a star surface, if one existed. They found little, if any, change of  $r_{in}$  at the transition to the intermediate spectral state. There was a dramatic decrease of the degree of ionization of the disk which they attributed to the disappearance of the soft component. In addition, they attributed a hardening of the power-law component to the decreased availability of soft photons for Compton cooling. A strong reflected component was found all the while the low state decline continued, which indicates that optically thick material was present within about 700 km throughout the observations that were analyzed. In all respects, these results exactly accord with expectations for a massive NS.

*GS 2000 + 25*: Życki, Done and Smith (1997a) have found a similar spectral state switch for GS 2000 + 25. When a strong soft component is present the disk is highly ionized and iron fluorescence strongly relativistically smeared. The disappearance of the soft component is accompanied by hardening of the power-law and a decrease of ionization. Little change of inner disk radius occurs at the transition, but the subsequent decline of luminosity is accompanied by an increase of inner disk radius. Using an inner radius of (50 - 100)  $R_g$  (1040 - 2080 km with  $R_g = 2GM/c^2$ ) as the co-rotation radius (Done, C. personal communication) and  $L_c = 1.5 \times 10^{35}$  erg/s for the hard state of Dec. 16, 1989,  $\nu_S = (4.5 - 1.6)$  Hz and  $B = (1.4 - 6.5) \times 10^{11}$  G are obtained. The calculated quiescent luminosity is  $(3.7 - 1.3) \times 10^{30}$  erg/s; well below the observational upper limit of  $2 \times 10^{32}$  erg/s.

*GS 2023 + 338* never displayed an ultra-soft spectral component, but on May 30, 1989 it changed luminosity by a factor of 21 in 10 s, from a saturated  $10^{39}$  erg/s to  $4.8 \times 10^{37}$  erg/s (Tanaka & Lewin 1995).  $10^{39}$  erg/s is the

Eddington limit for  $7 M_{\odot}$ . The iron fluorescence line was not obviously present in the high state but showed up prominently at the lower luminosity. This might be caused by a distended inner disk covering the magnetosphere. When the luminosity diminished, the reduction in the 1 - 10 keV band was greater than for higher energies. These phenomena strongly suggest that the magnetosphere expanded beyond the co-rotation radius when the luminosity dropped. Assuming this to be the case, apparently  $\Delta \approx 21$ . For  $7M_{\odot}$  and  $\Delta = 21$ ,  $u(R) = 0.56$ ,  $f_s + f_d(r_{ms}) = 0.428$  (Table 2), and  $f_d(r) = 0.02$ . Solving for  $u(r)$  yields 0.0434, which then gives  $r = 240$  km as the co-rotation radius. Using  $\dot{m} = L/f_d c^2$  with  $L = 4.8 \times 10^{37}$  erg/s gives  $\dot{m} = 2.7 \times 10^{18}$  g/s. Solving Eq. 14 for the magnetic field then yields  $9.5 \times 10^{10}$  G. The spin frequency (YM) determined from the co-rotation radius is 39 Hz.

From spectral analysis  $\dot{Z}ycki$ , Done and Smith (1997b) found  $r_{in} = 263$  km and 368 km, respectively, for June 20, 1989 and July 19-20, 1989. Luminosities (0.1 - 300 keV) for these dates based on spectra of Tanaka (1992) are  $1.9 \times 10^{37}$  erg/s and  $6.3 \times 10^{36}$  erg/s, respectively. These radii give values of  $f_d$  of 0.018 and 0.0134 and values of  $\dot{m}$  are then  $1.2 \times 10^{18}$  g/s and  $5.2 \times 10^{17}$  g/s. Values of  $B = 7.3 \times 10^{10}$  G and  $8.8 \times 10^{10}$  G then follow from Eq. 14. The three independent estimates of magnetic field are about as consistent as can be expected with an Eddington limit affecting the first result. Stated another way, if the  $9.5 \times 10^{10}$  G field is used with the values of  $\dot{m}$  to calculate the magnetospheric radii, values of 286 km and 365 km are found. These are within 9% of spectral fit values that have statistical uncertainties in excess of 50%.

Using the 39 Hz spin, the quiescent lu-

minosity would be  $(5.2 - 8.9) \times 10^{33}$  erg/s for  $(7.3 - 9.5) \times 10^{10}$  G. Quiescent luminosities of  $6.9 \times 10^{33}$  erg/s Chen, Shrader & Livio (1997),  $8 \times 10^{33}$  erg/s (Tanaka & Shibasaki 1996), and  $1.6 \times 10^{33}$  erg/s (Garcia, McClintock and Narayan 1997) have been reported. In any event, the calculated quiescent luminosity depends very strongly on spin, which is quite uncertain in this case with  $L_{min}$  so near the Eddington limit.

*1E1740.7-2942* is a jet source. Vilhu et al. (1997) fitted a "sombrero" model to a low state spectrum and found  $r_{in} \sim 7 - 8R_g$  for the  $10M_{\odot}$  they assumed. Taking this to be an inner radius of  $r_c = 225$  km and  $L_c$  to be the corresponding  $3 \times 10^{37}$  erg/s for  $7M_{\odot}$  yields  $\nu_S > 43$  Hz and  $B > 6.9 \times 10^{10}$  G. The hard spectrum with a small inner radius is incompatible with the advective accretion flow (ADAF) model of Narayan, Garcia and McClintock (1997). The calculated quiescent luminosity is  $< 7 \times 10^{33}$  erg/s.

*Cygnus X-1* has been observed to emit gamma rays (Ling et al. 1987). It exhibits spectral state switches with very little change of bolometric luminosity at about  $5 \times 10^{37}$  erg/s (Belloni et al. 1996). Misra & Melia (1997) obtained an inner disk radius of  $56.7 R_g$  from spectral fitting of an intermediate (hard) state. For  $10 M_{\odot}$ , this is 1700 km. Assuming this to be the co-rotation radius yields a spin frequency of 2.6 Hz. Using  $R = 14$  km in Eq 18 then yields  $B = 1.5 \times 10^{13}$  G. Magnetic fields of this magnitude have been associated with other gamma emitters such as the Crab and Vela pulsars. A lack of pulses would require nearly coincident rotation and magnetic axes and a lack of multipole moments. These are stringent, but not impossible, requirements. The calculated quiescent luminosity, should it ever be observed

for comparison, is  $1 \times 10^{33}$  erg/s.

*A0620 00:* Spectral hardening began about 100 days after the start of the 1975 outburst and continued until interrupted by a reflare.  $L_{min} = 8 \times 10^{36}$  erg/s (E. Kuulkers 1998) and  $L_q = 10^{31}$  erg/s (Garcia, Narayan & McClintock 1997) along with Eqs 18 and 22 permit the estimates,  $\nu_S = 13.5$  Hz and  $B = 2.3 \times 10^{10}$  G. The kinetic energy that the magnetosphere can impart to impinging matter is generally much less than the binding energy for the inner disk, but not for the light cylinder. This may be involved in the reflare process. In the case of Atolls and Zs, the spins are so fast that matter is too tightly bound at the light cylinder, hence little reflare is observed for them.

*GRO J1655-40:*  $L_{min}$  was reached at  $3.1 \times 10^{37}$  erg/s approximately July 29, 1996 (Mendez, Belloni and van der Klis 1998). The rapid decline was arrested at  $1.5 \times 10^{36}$  erg/s, which can be taken to be  $L_C$ . Eqs. 16 and 18 then yield  $\nu_S = 34$  Hz and  $B = 2.1 \times 10^{10}$  G. The calculated quiescent luminosity for these values exactly matches the observed  $2.5 \times 10^{32}$  erg/s reported by Garcia, McClintock & Narayan (1997).

*GRO J0422 + 32* never showed an ultrasoft peak and stayed in a spectrally hard, gamma emitting state during its 1992 outburst (Grove, et al. 1998). Lacking evidence of any spectral state change, only possible limits for spin and field can be estimated here. Using  $3.6M_\odot$ , (Chen, Shrader & Livio 1997) maximum luminosity  $7.9 \times 10^{37}$  erg/s as  $L_{min}$  and quiescent luminosity  $< 7.9 \times 10^{31}$  erg/s (Garcia, McClintock and Narayan 1997) as limits, one obtains  $\nu_S < 0.36$  Hz and  $B > 1 \times 10^{14}$  G. Such large magnetic fields may occur in nature, but it is possible that the spectrum might have remained hard for the same reasons, whatever they were, as SAX J1808.4-

3658. A slow spin would be consistent with the remarkable lack of high frequency features in the power density spectrum. This lack is at odds with accretion models that produce all hard x-rays and gamma emissions from regions near the innermost marginally stable orbit (Grove et al. 1998). Grove et al. found a strong QPO, independent of photon energy or luminosity at 0.23 Hz. If this is the spin frequency, the magnetic field could be as high as  $2 \times 10^{14}$  G. Another possibility is that the rapid decay after about  $10^{36}$  erg/s might correspond to the onset of the propeller effect. This would still imply a large magnetic field of  $10^{12}$  G. In either of these slow spin cases, the quiescent luminosity would be below  $5 \times 10^{31}$  erg/s; still below the observational upper limit.

*GRS 1915 + 105* displays oscillations with peaks above the Eddington limit followed by hard states that are lower in luminosity by a factor of 3 - 6. The conventional view is that the inner disk becomes unstable and a flare is produced by unspecified means as it falls into a black hole. Belloni et al. (1997) have attributed the intervals between flares to the time required for the inner disk to refill on a viscous time scale, which is likely correct. There is, however, a more credible explanation of the flares. They could arise from a star surface. If plasma falling from the innermost marginally stable orbit can produce a flare on the surface that is beyond the Eddington limit, radiation pressure could then push the disk back beyond this orbit and temporarily cut off the flow to the surface. After the inner disk refills, another flare follows, etc. MBB spectral fits (Belloni et al 1997) show that  $r_{in}$  oscillates between about 20 km and 80 km, but occasionally reaches only 55 km, followed immediately by another burst. 55

km would be the innermost marginally stable orbit radius (YM) for  $7M_{\odot}$ , which is therefore adopted as the mass.

A 67 Hz QPO has been observed (Remillard et al 1997, Remillard & Morgan 1998) that is sharp ( $Q > 20$ ), stable for factors of 5 luminosity change and stable over six months time. It is observed most clearly for luminosities for which surface radiations should be seen, if there is a surface. Speculating that this is the spin frequency, a co-rotation radius of 163 km (YM) is implied. The speculative 67 Hz spin frequency must be tested by further observations. There are two sources of drifts and broadening for this QPO. Orbital characteristics may imprint cyclical variations on it. Observing it at high luminosities with radial expansion of the surface layers may broaden it. If some of the hard secondary bursts that have been observed (Taam, Chen and Swank 1997) originate on the surface, as seems to be implied by the small radii determined for them, they may also show identifiable spin QPOs.

The low state between flares reached about  $4x10^{38}$  erg/s for a radius of about 80 km. Evaluating  $f_d$  for 80 and 163 km, calculating  $\dot{m} = 9.3x10^{18}$  g/s for the 80 km radius and scaling it for 163 km, ( $\alpha r_m^{-7/2}$ ) permits the calculation of  $L_c = 1.9x10^{37}$  erg/s. If the accretion rate of  $9.3x10^{18}$  g/s for the cutoff state were to impact the surface after refilling the inner disk, the luminosity could be driven to  $3.6x10^{39}$  erg/s, if not for the Eddington limit ( $\sim 10^{39}$  erg/s). The excess energy above the observed  $1.6x10^{39}$  erg/s may well be what drives the jets. In the 10 - 50 s durations of flares, excess energy of  $10^{40} - 10^{41}$  erg might be imparted to jets. The magnetic field, estimated from  $L_c$  and Eq. 16 is  $2.8x10^{10}$  G. It is noteworthy that this exceeds the minimum

$10^8$  G found by Gliozzi, Bodo & Ghisellini (1998) to be necessary for the field strength at the base of the jets of GRS 1915+105.

Eq 22 yields an expected quiescent x-ray luminosity of  $7x10^{33}$  erg/s. In all parameters, GRS 1915 + 105 seems to be like GRO J1655-40 and Cir X-1, both of which are also chaotically variable in both x-ray and radio regimes. It should be clear from the low value of  $L_c$ , that accreting mass should have reached the surface at all times for the observed oscillation luminosities under consideration. That it apparently did not, judging by the hard spectrum after a burst, is due to the empty inner disk after the burst. The star behaves as a relaxation oscillator between the super-Eddington flares and innermost marginally stable orbit. For oscillations, it is critical that the magnetic field be of the right strength to just require flows near the Eddington limit to drive the magnetosphere near the marginally stable orbit. Massive stars with very large surface efficiencies can then provide a strong burst as mass hits the surface. The oscillating state might require a balance of fields and accretion rates too delicate for achievement by low mass neutron stars that have no accretion gaps.

## 5. Spectra of Massive NSs

For this discussion it must be remembered that there are only two reliable distinguishing spectral characteristics of BHCs. These are the simultaneous presence of hard spectral tails and ultrasoft spectral components above  $10^{37}$  erg/s and larger amplitude flickering for some BHCs. Both are indicators of larger masses for BHCs in the massive NS model. No event horizon explanation has been proposed for them for black hole models. Flickering can be explained by shot penetrations

of the magnetopause, as illustrated by the flickering pulsar, VO332+53. A shot mechanism has the virtue of being able to account for the strong coherence (Nowak et al. 1998) of soft and hard emissions during flickering. Stronger flickering of the BHCs is due to their larger surface binding energies. The quenching of the hard spectral tail of the low mass NSs is due to the fact that  $10^{37}$  erg/s is a much larger fraction of the Eddington limit for low mass NSs. At this and higher luminosities, radiation pressure inflates the inner disk and the flood of soft photons cools the Comptonization region. The magnetosphere would not be inside the co-rotation radius for many BHCs at  $10^{37}$  erg/s. These would automatically have hard spectra at this luminosity.

Three separate regions contribute to the spectra of NSs. These are the surface and co-rotating magnetosphere, the inner disk-magnetopause, and the outer disk. It is accepted that blackbody and/or thermal brehmsstrahlung spectra of  $kT_{bb} \sim 2$  kev arises from the region near the surface. Hard power-law radiations seem to come from the inner disk-magnetopause region, and soft excess thermal radiations  $kT_{bb} \sim 0.1 - 0.6$  kev originate from the outer disk. Not only are these spectrally different regions, they have been spatially resolved in dip observations. Morley et al. (1998) have analyzed deep (100%) dips in the high state spectrum of XB 1916-053 to show that  $kT_{bb} = 1.95$  keV blackbody emissions arise from a rapidly covered central NS while a strong power-law spectrum beyond 100 kev with photon index of 1.75 was produced by a larger emission region. Observations of hard, low states show dominant power-law spectra along with a low temperature soft excess that produces a few percent of the luminosity.

Exactly the same spectral features and some of the same spatial features have been observed for BHCs. For BHCs, however, the strong soft radiations are attributed to the disk and are usually represented by MBB radiation functions. It is a stroke of good fortune that MBB functions represent the central soft sources of both NSs and BHCs, but certainly no proof of an event horizon. A similar analysis of high state dips of the BHC GRO J1655-40 (Kuulkers et al. 1997) revealed a bright, but unresolved central region that produced a power-law and a MBB of 1.1 kev temperature. The entire x-ray emitting region was found to be smaller than  $\sim 460$  km. The disk diameter at the co-rotation radius found here for this source would be 550 km. The inner disk would have to be smaller than this for a NS to produce the high state. In a similar way, the times of ingress and egress for dips of Cygnus X-1 (Kitamoto et al. 1984) constrain the size of the region of origin of its low state hard spectrum to be of order 4000 km for luminosities for which the disk inner diameter would be near 3400 km (Misra & Melia 1997).

Thus the inner disk-magnetopause region is a likely site of hard photon production. This would be consistent with the large solid angles relative to the disk seen for reflected x-rays as disk radii expand in decline. Zhang, Yu & Zhang (1998) have suggested that flow reversal at the magnetopause could produce a hard power-law spectrum by the same bulk Comptonization mechanism examined by Kluzniak & Wilson (1991), Hanawa (1991), and Walker (1992) for flow into a boundary layer. Whether or not flow reversal bulk Comptonization or magnetospherically driven return flows (Arons et al. 1984) are related to the hard spectrum, the energy requirements

for the power-law strongly suggests that it would have to originate in the inner disk.

For both Cygnus X-1 (Balucinska-Church et al. 1997) and GRO J1655-40, (Kuulkers et al. 1997) a soft excess was found to comprise  $\sim 6\text{-}8\%$  of disk emissions. It was modeled as a blackbody in both cases. Temperatures of 0.13 keV and 0.60 keV, respectively, were found for the soft excesses of the two sources. Balucinska-Church et al (1995) identified the soft excess as disk emissions. The relatively stronger presence of the soft excess in the deeper dips of GRO J1655-40 confirms that they must arise from the outer disk. It is unlikely that all of the gravitational binding energy available from the outer disk is used in producing a soft excess luminosity. The soft excess is quite small compared to the power-law which also originates in the disk. However if the fraction of binding energy that produces the soft excess is roughly independent of radius, the disk temperature will still scale as  $T \sim r^{-3/4}$ . The temperature of 0.13 keV for Cygnus X-1 at 1700 km scales up to 0.58 keV at the 230 km of GRO J1655-40. This provides additional confirmation of the outer disk as the source of much of the soft excess.

An ultrasoft spectrum was first recognized for BHCs by White & Marshall (1984) for LMC X-1 and LMC X-3. Analysis of Rossi observations (Wilms et al. 1998) of these persistent, high state sources have shown that their spectra can be fitted with a MBB (or blackbody as well for LMC X-1) of temperature,  $kT_{bb} = 1.0$  and 1.25 keV, respectively for these sources, along with a power law. A  $5\text{-}9 M_{\odot}$  Yilmaz NS emitting as a blackbody would have a surface redshift of  $z \sim 0.5\text{-}2.4$  (Fig. 1, Table 2). A local surface temperature of 2.3 keV would produce a distantly observed apparent temperature of  $T/(1+z) =$

2 keV for a low mass NS and 1.3 - 0.7 keV for the BHC. Thus bright, ultrasoft peaks are well explained for massive NSs.

We conclude that all of the distinguishing characteristics of BHCs are encompassed by the massive NS hypothesis. If a suitable model for NSs were available, we might apply it with some confidence to the BHCs. Unfortunately, none is available. Blackbody or thermal brehmsstrahlung might be expected from near the star surfaces. Such simple models (as well as apparently inappropriate high temperature MBBs) do a fair job of representing the soft spectral components of both BHCs and low mass NSs. What is lacking is an understanding of the power-law emissions. They so dominate the low state spectra, leaving only small soft excesses, that an optically thick, viscosity dominated disk (with its associated lower temperature MBB spectrum) may not be an adequate starting point for the hard x-ray spectrum. It is not certain that an optically thick disk at the temperature of the soft excess could generate a sufficiently energized corona to produce the power-law component.

The low state disk may be optically thin for x-rays and/or advective, i.e., not dominated by viscosity. An advective accretion flow (ADAF) model was proposed (Narayan et al 1997) to explain the hard quiescent radiations of BHCs. In this model, the disk is optically thin and very hot, and accretion rates above  $10^{15\text{-}16}$  g/s are needed to produce quiescent luminosity. According to Eq. 14, Atoll sources with magnetic fields of  $\sim 2 \times 10^8$  G would have magnetospheric radii of 50 - 100 km for these accretion rates (or less, accepting Dong Lai's suggestion). With spins of  $\sim 350$  Hz they would produce  $\sim 5 \times 10^{34\text{-}35}$  erg/s for these accretion rates without any

surface contributions and much more unless propeller effects block surface emissions completely. Since quiescent luminosities of Atolls are far below these levels, the high accretion rate ADAF model is simply inapplicable to quiescent NSs. Recall that ADAF models with transitions to the conventional optically thick, geometrically thin, disk (Esin, McClintock & Narayan 1997) at radii beyond  $10^4 R_g$  have been shown (Życki, Done & Smith 1997) to fail for BHCs as well. Finally, the presence of a hard spectrum for 1E1740.7-2942 for an inner disk radius of only 225 km shows that the ADAF model simply cannot be taken seriously. While there seems to be little to recommend pure ADAF models, a combination of partially advective and magnetospheric effects cannot be ruled out. An advective disk with a magnetospherically driven return flow (Arons et al. 1984) might have some merit. Advective flows can have positive energy for the return.

The nature of the spectrum that would arise from within the magnetosphere for luminosities above  $L_c$  is also unclear. The production of soft photons via cyclotron emission would be difficult to quantify. The spectrum of photons arising from the surface might be blackbody or thermal brehmsstrahlung. Psaltis, Lamb & Miller (1995) have calculated spectra and successfully reproduced the color-color diagram for a Z-source with an accretion disk-central corona-magnetosphere model. It is possible that this model might be extended to encompass the hard spectrum of the propeller regime, for which the hot corona might be located at the magnetopause. The hard spectrum of SAX J1808.4-3658 illustrates an additional difficulty for spectral models. The emergent observed spectrum may be strongly affected by inclination effects.

Black hole models must necessarily use an optically thick disk to produce soft peaks and some Comptonization of soft photons to produce power-laws. Although current models with central black holes and accretions disks have had some success in representing static spectra for some states of the BHCs, most models rely on features such as a hot central corona introduced in a purely *ad hoc* fashion. It remains to be shown rigorously that a hot central corona would develop for Keplerian flow into an event horizon. The current "sombroero" models (Poutanen 1998) do a good job of representing some BHC spectra but require that the accretion disk intrusion into the central corona be "just so" to let just the right number of seed photons be Compton scattered to produce the hard spectrum. It is not clear that such a model can account for the timing signatures within the spectrum.

## 6. Active Galactic Nuclei

It must be acknowledged that active galactic nuclei pose an interesting challenge for any alternative theory of gravity. Spectral state switches have been observed for them (Mannheim et al 1995). They likely do not possess star cluster cores (Maoz 1995). Massive single objects with accretion disks might be possible but they would be most unusual astronomical objects. It can be readily seen from Eqs. 11 and 12 that a mean density of  $\sim 1g/cm^3$  could correspond to a very compact object of  $\sim 10^8 M_\odot$  that would not necessarily be a black hole, even in SM. Given the extremely high efficiency of conversion of gravitational mass-energy to luminosity, there should be no problem modeling AGN levels of radiation. But the constant proper density model is wholly inadequate. Realistically, an object of such low density might need

to be supported internally by radiation pressure (but see Gruber 1998) and would likely have large density gradients and strong magnetic stresses. This is clearly a topic for another time, but one that should be pursued. Black holes would certainly be simpler, but we should confirm them among the galactic BHCs, where we can strongly constrain masses and radii, if at all possible. The issue is clearly that of the existence or non-existence of an event horizon. YM objects with  $u(R) > 1/2$  are more compact than black holes of the same mass and might well be of low luminosity with their surfaces inside the photon orbit.

## 7. Conclusions

The characteristics of BHCs appear to be compatible with a massive NS model. The signatures of this model are strong magnetic fields, large surface binding energies and large redshifts of surface emissions. The field can produce power-law and gamma emissions, jets, spectral state switches and cyclotron emissions and the surfaces can produce ultrasoft peaks and large rms flickering. The magnetic field strengths and spins proposed here for BHCs are reasonably near the spin-up trend line from radio pulsars to millisecond pulsars. Where co-rotation radii can be determined from spectral fit parameters, the corresponding spin rates and subsequently found magnetic field strengths imply quiescent luminosities in agreement with observations. Due to their slower spins, the magnetospheric contributions to the quiescent luminosities of the BHCs appear to be somewhat smaller than those of the low mass Atoll and Z NSs. The work of  $\dot{Z}$ ycki, Done and Smith (1998a) describes a spectral state switch in exact accord with the magnetic propeller mechanism

cutting off the flow to the surface with little change of inner disk radius. Cir X-1, the NS most like a BHC, has been found to have spin and magnetic field similar to many of the BHCs. The ubiquitous slow  $\sim 6$  Hz QPOs found in high states of both BHCs and NSs (Miyamoto, Kimura & Kitamoto 1991, Makishima et al. 1986), can be explained as accretion disk flow and opacity oscillations driven by surface radiations (Fortner, Lamb & Miller 1989). It is not known how a black hole might produce them.

A clear implication of the massive NS model is that hard spectral features arise from the inner disk (magnetopause?) while soft spectral features can arise from both the disk and the surface. The strong reflected x-rays seen in hard states with fairly large solid angles subtended as the disk radius expands in decline, suggests that the magnetopause might be a primary site of hard photon production.

Adoption of the massive NS hypothesis would eliminate many difficulties for accretion disk theory. Spectral state switches would no longer require discontinuous disk behavior for transitions between high and low states. An additional burden for disk theory is removed by no longer requiring disk explanations for occasional BHC failures to produce ultrasoft peaks at high luminosities. The massive NS hypothesis explains these as either magnetic axis orientation effects or failure of the inner disk to penetrate the co-rotation radius. The structure of the transition region near the magnetopause is likely to be much more complex than previously implied here. It is likely to be involved in a complicated, inclination dependent way in the production of the pairs of kHz QPOs.

Three of the BHC cases examined here, including Cyg X-1, seem to have spins below

10 Hz and very strong magnetic fields. All are above the "death line" for pulsars, while V0332+53, the original flickering pulsar, is not. Cyg X-1 is a wind accreter that appears to be delicately balanced between intermediate and low states. Its large co-rotation radius permits a large energy release and consequent large radiation pressure increase when mass does reach the star surface. The net effect is a somewhat self-regulated luminosity. It is likely near spin secular equilibrium, as are the Zs and Atolls. Aside from their spins being revealed during bursts, the Zs and Atolls are not x-ray or radio pulsars. Magnetic fields of order  $10^{10}$  G and higher may be sufficient to suppress bursts, however, Cir X-1 has exhibited bursts. The similarly weak magnetic fields of GRO J1655-40, A0620-00 and GRS 1915+105 suggests that they should be carefully monitored for bursts; indeed this last source may have already produced some (Taam, Chen, & Swank 1997). That the stronger-field BHCs are not bursters would be expected. The lack of pulses requires near-coincident magnetic and spin axes or extreme magnetic fields. Such a configuration is likely necessary for efficient production of jets and may enhance gamma emissions.

KHz QPOs corresponding to the Keplerian frequencies of the inner disk imply that the accretion disks of both NSs and BHCs can reach to near the innermost marginally stable orbit. With a fixed binding energy for this orbit it seems clear that we must look for the differences between NSs and BHCs inside this orbit. Black hole disk models that are differentiated from NS disks without explicitly incorporating the differences between event horizons and star surfaces should have little credibility.

A tremendous amount of detailed model-

ing will be necessary to extend the massive NS hypothesis beyond this introduction. The Yilmaz modifications of general relativity have provided an acceptable basis for the explorations of the differences between surfaces and event horizons. The simplicity of the Yilmaz theory, both mathematically and conceptually, warrants its continued use. Its strong metric similarities to general relativity below  $2M_{\odot}$  and the lack of an event horizon beyond  $3M_{\odot}$  will provide for stringent comparisons of black hole vs NS models. The recent discovery of NSs of approximately  $2 M_{\odot}$  (Zhang et al. 1998) should permit detailed comparisons of the two theories for NSs in a range where differences might first appear. For example, the amplitudes of QPOs generated from bursts might be expected to differ due to differences of gravitational curvature of photon trajectories. Comparisons of this sort might be complicated for masses large enough for the surfaces to be inside the photon orbit. The important point, however, is that the Yilmaz metric provides a sharp tool that should eventually decide the question of the existence of event horizons.

## 8. Acknowledgements

It is a pleasure to acknowledge many stimulating and helpful discussions with my colleagues, Ray C. Jones, Adam Fisher and Charles Rogers. The encouragement of Prof. Carroll O. Alley, University of Maryland and a manuscript review by Darryl Leiter are also appreciated. I am indebted to Adam Fisher for technical assistance. A great debt is owed to those whose dreams produced x-ray vision and who have told us what they have seen.

## Appendix 1. Particle Mechanics

The mechanics of a particle orbit can be examined very simply with the aid of the energy-momentum four-vector. The magnitude of this vector, given by  $g^{ij}p_i p_j$ , is  $m_0^2 c^2$  where  $m_0$  is the rest mass of the particle. For a particle in an equatorial orbit ( $\theta = \pi$ ,  $p_\theta = 0$ ) about an object of gravitational mass  $M$  in the SM, one obtains:

$$\frac{E^2}{(1-2u)c^2} - (1-2u)p_r^2 - \frac{p_\phi^2}{r^2} = m_0^2 c^2 \quad (1)$$

Here  $p_0 = E/c$ , where  $E$  is the particle energy and  $u = GM/c^2r$  is the gravitational potential at distance  $r$  from the center of mass  $M$ .  $p_\phi$ , the particle angular momentum, is a constant of the motion. Further, by defining  $a = (cp_\phi/GMm_0)$  and rearranging, the equation above becomes:

$$(1-2u)^2 \frac{p_r^2}{m_0^2 c^2} = \frac{E^2}{m_0^2 c^4} - (1-2u)(1+a^2 u^2) \quad (2)$$

For suitably small energy, bound orbits occur. Turning points for which  $p_r = 0$  can be found by examining the effective potential, which consists of all terms to the right of  $E^2/m_0^2 c^4$  above. At minima of the effective potential we find

$$a^2 = \frac{1}{u - 3u^2} \quad (3)$$

and with  $p_r = 0$ , we get

$$E = m_0 c^2 \frac{(1-2u)}{\sqrt{(1-3u)}} \quad (4)$$

The innermost marginally stable orbit is found by setting the first two derivatives of the effective potential with respect to  $u$  to zero. This gives the well-known results,  $u = 1/6$  and  $a^2 = 12$ . With this value of  $u$ ,  $E = \sqrt{(8/9)} m_0 c^2$ .

Substituting this value for  $E$ , the radial motion equation for a subsequent geodesic fall to the star surface is:

$$(1-2u) \frac{p_r^2}{m_0^2 c^2} = \frac{1}{9}(6u-1)^3 \quad (5)$$

Equating  $p_r$  to  $mv_r$ , using  $m = E/c^2$  and recognizing  $(1-2u)v_r$  as the proper velocity at the position where the potential is  $u$ , the radial velocity relative to a distant observer is seen to be

$$v'_r = \frac{\sqrt{2}}{4} c (6u-1)^{3/2} \quad (6)$$

Analogous treatment of the orbit equation in the YM yields:

$$\exp(-4u) \frac{p_r^2}{m_0^2 c^2} = \frac{E^2}{m_0^2 c^4} - \exp(-2u)(1+a^2 u^2 \exp(-2u)) \quad (7)$$

Setting the first two derivatives of the effective potential to zero in this case produces coupled equations which have a solution for  $u = (3 - \sqrt{5})/4 \approx 0.191$  with  $a^2 = 12.4$ . Circular orbits occur for

$$a^2 = \frac{\exp(2u)}{u - 2u^2} \quad (8)$$

and

$$E = m_0 c^2 \exp(-u) \sqrt{\frac{1-u}{1-2u}} \quad (9)$$

A particle in geodesic infall starting with  $p_r = 0$  at the marginally stable orbit would arrive at the star with velocity components:

$$v'_r = c[1 - 1.12 \exp(-2u)(1 + 12.4u^2 \exp(-2u))]^{1/2} \quad (10)$$

$$v'_\phi = 3.73 c u \exp(-2u) \quad (11)$$

The radial velocity is supersonic for disk temperatures of as much as 1 keV for  $u = 0.2$ ; i.e., for very little change of potential relative to

that of the marginally stable orbit. For  $u = 0.25$ , corresponding to the surface of a star of  $\approx 3 M_\odot$ , the radial speed for a Keplerian fall from the marginally stable orbit would be about  $10^9$  cm/s.

The Keplerian frequency of the marginally stable orbit can be found from the relations:  $\nu_K = \frac{1}{2\pi} \frac{d\phi}{dt} = \frac{g\phi p_\phi}{2\pi m_0 c} \frac{ds}{dt}$ ,  $p_\phi = \frac{GMm_0 a}{c}$  and  $ds = \frac{m_0 c^3}{E} \exp(-2u)$  to be:

$$\nu_K = \frac{\sqrt{GM} \exp(-2u)}{2\pi r^{3/2} \sqrt{1-u}} \quad (12)$$

In either metric there is an unstable circular photon orbit. In the YM this lies outside the star surface for  $u(R) > 1/2$ , or for  $m_g > 6 M_\odot$ . For black holes the unstable photon orbit occurs for radius  $r = 1.5 R_s$ . Although radially directed photons can always escape in the YM, those with too much orbital angular momentum can be trapped inside the unstable photon orbit.

## 2. Compact Objects

The constant proper density object is one of *constant intrinsic local density*. Since there are cases of interest for extensions of this model to variable local density, the appropriate equations will be set up for a more general case. Consider a spherically symmetric density distribution  $\rho_0 h(r < R)$  with  $\rho_0$  a constant and  $h(r)$  a distribution function for local density. The condition  $h(0) = 1$  is imposed without loss of generality, and all mass is confined within radius  $R$  relative to a distant observer. In this model, the proper density,  $\rho(r)g(r)$  is assumed to be given by  $\rho_0 h(r)$ . Thus it will be assumed that  $\rho(r) = \rho_0 h(r)/g(r)$ . As shown by Clapp (Clapp 1973),  $u(r)$  can be constructed by adding the potentials of successive shells of matter. Inside each shell the

contribution to  $u(r)$  is constant and outside it declines as  $1/r$ . For a general radius  $r$ , with  $r < R$ , contributions to the potential must be separated into those arising from shells of radius  $r'$  inside  $r$  and those from shells of radius  $r'$  outside  $r$ . The gravitational mass within each shell is  $4\pi r'^2 \rho_0 h(r') dr'/g(r')$ . (For the free baryon mass substitute  $g(r')^{3/2}$ .) The central potential  $u(0)$  is obtained by dividing each shell mass increment by  $r'$  and integrating out to  $R$ . Subtracting  $u(0)$  from  $u(r < R)$  leads to Clapp's integral equation:

$$u(r < R) - u(0) = \frac{-4\pi G \rho_0}{c^2} \int_0^r dr' h(r') (r' - r'^2/r)/g(r') \quad (13)$$

It can be shown that this equation is a solution of the field equations of either gravitational theory by substitution of the appropriate  $g(r)$  and other metric components into the field equations and solving the  $G_{tt}$  differential equation for  $u(r)$ . By expressing  $u(r < R)$  and  $u(0)$  in terms of  $g(r)$  and  $g(0)$  and incorporating  $g(0)$  into a scale factor for lengths, the integral can be recast in the dimensionless form:

$$y(x) = -2 \int_0^x f(x') h(x') (x' - x'^2/x) dx' \quad (14)$$

where  $x = r/(r_0 g(0)^{N/2})$ ,  $r_0 = c/\sqrt{4\pi G \rho_0}$ ,  $f(r) = g(0)/g(r)$ ,  $N = 1$  in the YM and  $N = 2$  in the SM. Thus these collapsed objects can be described with the aid of the characteristic radius,  $r_0$ , and a characteristic mass,  $M_0 = c^2 r_0/G$ . In the exponential metric:

$$y(x) = \ln(f(x)) \quad (15)$$

and in the SM:

$$y(x) = 1 - 1/f(x) \quad (16)$$

After substituting the appropriate left member, the integral equation can be numerically solved for  $f(x)$  by an iterative relaxation

method starting from  $f(x) = 1$  for  $x < 1$  and an asymptotic value for  $x > 1$ . Asymptotic solutions for the constant intrinsic density model, for which  $h(r) = 1$  are  $f(x) = x^{-2}$  for the YM, (Clapp 1973) and  $x^{-1}$  found here for the SM. Physical quantities such as gravitational mass  $m_g$ , equivalent free baryon mass,  $m_b$ , distantly observed red shift of surface radiations,  $z$  and radius,  $R$  can be expressed in terms of certain integrals over  $f(x)$ . Following Clapp (Clapp 1973), these are:

$$F_1(x) = \int_0^x h(x')f(x')x'dx' \quad (17)$$

$$F_2(x) = \frac{1}{x} \int_0^x h(x')f(x')x'^2dx' \quad (18)$$

$$F_3(x) = \frac{1}{x} \int_0^x f(x')^{3/2}x'^2h(x')dx' \quad (19)$$

In the exponential metric there follows:

$$m_g = M_0xF_2(x) \exp(-F_1(x)) \quad (20)$$

$$m_b = M_0xF_3(x) \quad (21)$$

$$R = r_0x \exp(-F_1(x)) \quad (22)$$

$$u(0) = F_1(x) \quad (23)$$

$$u(R) = F_2(x) \quad (24)$$

In the SM the same quantities are given by:

$$m_g = M_0 \frac{xF_2(x)}{(1 + 2F_1(x))^2} \quad (25)$$

$$m_b = M_0 \frac{xF_3(x)}{(1 + 2F_1(x))^{3/2}} \quad (26)$$

$$R = r_0 \frac{x}{(1 + 2F_1(x))} \quad (27)$$

$$u(0) = \frac{F_1(x)}{1 + 2F_1(x)} \quad (28)$$

$$u(R) = \frac{F_2(x)}{1 + 2F_1(x)} \quad (29)$$

Numerical solutions of Eq. 14 and the appropriate integrals for the case  $h(r) = 1$  were used to generate the data of Table 2 and Table 3. Plots of mass, radius and redshift for surface emissions are shown in Figures 1 and 2. Choosing  $h(r) = 1$  forces the object to be of *constant local intrinsic density*. To an external observer, there would be substantial variations of density, but locally everything would seem entirely normal. Such is life in radically curved space-time. Simple extensions of this approach to an Oppenheimer - Volkoff method for the determination of  $\rho_0$  and  $h(r)$  are possible, as well as exponential atmosphere models of active galactic nuclei ( $h(r)$  not equal to 1), but the essential differences between black holes, neutron stars and nuclear-density compact objects in the exponential metric are clearly revealed by this simple model.

## REFERENCES

Alley, Carroll O. in Fundamental Problems in Quantum Theory, Annals New York Academy of Sciences 1995, 755, 464

Arons, J. et al. 1984, in AIP Conference Proceedings No. 115, High Energy Transients in Astrophysics, p. 215, American Institute of Physics, New York

Bailyn, C., Orosz, J., McClintock, J. & Remillard, R. 1995 *Nature* 378, 157

Balucinska-Church, M., Belloni, T., Church, M. & Hasinger, G. 1995 *astro-ph/9509020*

Balucinska-Church, M., Takahashi, T., Ueda, Y., Church, M., Dotani, T., Mitsuda, K. and Inoue, H., 1997 *ApJ*, 480, L115

Barret, D. et al. 1992 *ApJ.*, 394, 615

Barret, D., McClintock, J., & Grindlay, J., 1996 *ApJ*, 473, 1996

Bhattacharya D., & Srinivasan, G., 1995 in "X-Ray Binaries", eds W. Lewin, J. van Paradijs & E. van den Heuvel, Cambridge Univ. Press

Becker, W. and Trümper, J. 1997 /9708169

Belloni, T. et al. 1996 *ApJ* 472, L107

Belloni, T. et al. 1997 *ApJ* 488, L109

Bradt, H., Shirey & Levine 1997 Proc. of "The Active X-Ray Sky: Results from Beppo-Sax and Rossi-XTE", Nuclear Physics B Supp., eds L. Scarsi, H. Bradt, P. Giommi & F. Fiore, Rome /9801259

Brown, E., Bildsten, L. & Rutledge, R. 1998 *ApJ* 504, L95, 1998

Campana, S. et al. 1998a /9805079

Campana, S. et al. 1998b *ApJ* 499, L65 /9803303

Casares, J., Charles, P. & Kuulkers, E. 1998 *ApJ* 493, L39

Chen, W., Shrader, C. & Livio, M. 1997 *ApJ* 491, 312

Churazov, E., et al., 1995, *Apj.* 443, 341

Clapp, R. E., 1973 *Phys. Rev. D* 7, 345

Corbet, R. 1996 *ApJ* 457, L31

Cui, W. 1997 *ApJ* 482, L163

Cui, W., Morgan, E. & Titarchuk, L., 1998 *ApJ* 504, L27

Dower, R., Bradt, H. & Morgan, E. 1982 *ApJ* 261, 228

Ebisawa, K. et al., 1994 *PASJ*, 46, 375

Einstein, A. in "The Collected Papers of Albert Einstein, v.2., The Swiss Years: Writings 1900 - 1909", p. 457, Princeton University Press (1989)

Esin, A., McClintock, J. & Narayan, R. 1997 *ApJ* 489, 865

Fortner, B., Lamb, F. & Miller, G., 1989 *Nature* 342, 775

Friedman, J. & Ipser J., 1987 *ApJ*, 314, 594

Garcia, M., McClintock, J. & Narayan, R. 1997 /9708149

Ghosh, P. & Lamb, F. 1992 in X-Ray Binaries and Recycled Pulsars, Ed. E. van den Heuvel and S. Rappaport, Kluwer

Gilfanov, M. et al. 1998 /9805025

Gliozzi, M., Bodo, G. & Ghisellini, G. 1998 *MNRAS*, *astro-ph/9810029*

Graber, J. 1998, *astro-ph/9712197*

Grove, J. et al. 1998 /9805256

Halpern, J. & Wang, F. 1997 *ApJ* 477, 905

Hameury, J., Lasota, J., McClintock, J. & Narayan, R. 1997 *ApJ* 489, 234

Hanawa, T., 1991 ApJ, 373, 222

Heindl, W.A. & Smith, D.M., 1998 /9805372

Illarianov, A. & Sunyaev, R. 1975 A&A 39, 185

Kalogera, V. & Baym, G., 1996 ApJ. 470, L61

Kitamoto S. et al. 1984 PASJ 36, 731

Kluzniak, W. & Wilson, J., 1991 ApJ, 372, L87

Kusunose, M., Minishige, S. & Yamada, T., 1996 ApJ, 457, 813

Kuulkers E. et al. 1998 ApJ in press, astro-ph/9710024

Kuulkers, E. 1998 in New Astronomy Reviews, in press /9805031

Lai, D. 1998 /9711142

Lamb, F., Pethick, C. & Pines, D. 1973 ApJ 184, 271

Ling, J., et al., 1987 ApJ 321, L117

Mannheim, K. et al, 1995 /9512045

Maoz, E. 1995 ApJ 447, L91

Mendez M., Belloni, T. and van der Klis, M. 1998 ApJ 499, L000

Michel, F.C. 1991 in "Theory of Neutron Star Magnetospheres, Univ. Chicago Press, Chicago, Ill.

Miller M., Lamb, F. & Psaltis, D. 1997 ApJ, in press /9702090)

Miller, M. 1998 ApJ Lett., under review /9809235

Misra, R. & Melia, F. 1997 ApJ 484, 845

Makishima, K. et al., 1986 ApJ 308, 635

Mitsuda, K., Inoue H., Nakamura, N & Tanaka, Y. 1989 PASJ 41, 97

Miyamoto, S., Kimura, K., & Kitamoto, S., 1991 ApJ 383, 784

Miyamoto, S., Kitamoto, S., Mitsuda, K., & Dotani, T., 1988 Nature, 336, 450

Miyamoto, S., Kitamoto, S., Iga, S., Negoro, H. & Terada, K., 1992 ApJ 391, L21

Morley, R., Church, M, Smale, A. & Balucinska-Church, M. 1998 MNRAS in press, astro-ph/9810185

Narayan, R., Garcia, M., McClintock, J., 1997 ApJ. 478, L79

Nowak M. et al. 1998 ApJ in press (astro-ph/9712106)

Orosz, J., Remillard, R., Bailyn, C. & McClintock, J. 1997 ApJ 478, L83

Pan, H., Skinner, G., Sunyaev, R. & Borozdin, K., 1995, MNRAS, 274, L15

Poutanen, J. 1998 in Theory of Black Hole Accretion Disks, eds M. Abramowicz, G. Bjornsson & J. Pringle, Stockholm Observatory High Energy Astrophysics Preprint #8

Remillard, R. et al /9705064

Remillard, R. & Morgan, E. 1998 /9805237

Rindler, W. in Essential Relativity, 1969 Van Nostrand Reinhold Co., Canada, p. 146

Shibata et al. 1997 ApJ 483, 843

Singh, K., Apparao, K. & Kraft, R., 1994 ApJ, 421, 753

Stella, L., et al. 1985 ApJ, 288, L45

Stella, L., White, N. & Rosner, R. 1986 ApJ 308, 669

Strohmayer, T. et al. 1998 ApJ. 498, L135

Sunyaev, R. & Trümper, J., 1979 Nature 279, 506

Swank, J. 1998 /9801218

Taam, R., Chen, X. and Swank, J. 1997 ApJ, 485, L83

Taam, R. & Picklum, R., 1978 ApJ, 224, 210

Tanaka, Y. in 1992 Ginga Memorial Symposium, Ed. F. Makino and F. Nagake

Tanaka, Y. & Lewin, W. 1995 in "X-Ray Binaries", eds W. Lewin, J. van Paradijs & E. van den Heuvel, Cambridge Univ. Press

Tanaka, Y. & Shibasaki, N., 1996 ARA&A, 34, 607

Tennant, A., Fabian, A. & Shafer, R., 1986 MNRAS, 221, 27p

van der Klis, M., 1994 ApJ. SS92, 511

van der Klis, M. 1996 Proc. NATO Advanced Study Institute, "The Many Faces of Neutron Stars", Lipari, Italy /9710016

Vilhu, O. et al /9707094

Walker, M., 1992 ApJ., 385, 661

White, N. & Marshall, F., 1984 ApJ, 281, 354

White, N., Stella, L. & Parmar, A., 1988 ApJ, 324, 363

White, N. & Zhang, W. 1997 ApJ 490, L87

Will, C. 1981, Theory And Experiment in Gravitational Physics, Cambridge University Press

Wilms, J., et al., 1998 ApJ, in press, astro-ph/9810077

Yilmaz, H., 1958, Phys. Rev., 111, 1417

Yilmaz, H., 1971, Phys. Rev. Let., 27, 1399

Yilmaz, H., 1975, Am. J. Phys., 43, 319

Yilmaz, H., 1981, Physics Today, Letters, October, p.107

Yilmaz, H., 1992, Il Nuovo Cimento, 107B, 941

Yilmaz H., 1994, in Frontiers of Fundamental Physics, Ed. M. Barone & F. Selleri, Plenum Press, New York, p. 115

Yilmaz H., 1995, in Fundamental Problems in Quantum Theory, Annals New York Academy of Sciences 1995, 755, 477

Zhang, W. et al, 1997 ApJ 479, 381

Zhang, W., Yu, W. & Zhang, S. 1998 ApJ 494, L71

Zhang, W., Smale, A.P., Strohmayer, T.E. & Swank, J. H. 1998 ApJ 500, L171

Życki, P., Done, C. and Smith, D. 1997a /9712190

Życki, P., Done, C. and Smith 1997b ApJ 488, L113

Życki, P. Done, C. & Smith, D. 1998 ApJ 496, L25

TABLE 1  
NEUTRON STAR PROPERTIES

Object	$L_{min,36}$	$L_{c,36}$	$L_{q,33}$	$M (M_{\odot})$	$R$ (km) <sup>a</sup>	$\nu_S$ (Hz)	$B_9$ (G)	References.
Neutron Stars (Pulsars)								
V0332+53	0.07			1.4	15	.227	270	12
PSR GX 1+4				1.4	15	0.0083	31000	13
PSR GRO J1744-28	1.8			1.4	15	2.14	103	tw, 13
PSR 1055-52			0.2	1.4	15	5	1500	tw, 32
Sax J1808.4-3658	1.5	0.4	0.17 <sup>a</sup>	1.4	15	401 <sup>b</sup>	0.21 <sup>a</sup>	1, 2
Neutron Stars (Atoll)								
Aql X-1	1.2		0.4	1.4	15	549 <sup>b</sup>	0.13 <sup>a</sup>	3, 4, 20
4U 1608-52	10		2	1.4	15	460 <sup>b</sup>	0.46 <sup>a</sup>	7, 20, tw
4U 1820-30	15		1-3.4 <sup>a</sup>	1.9	15	275-550 <sup>b</sup>	0.5-1.1	5, 6
4U 1730-335	10		2	1.4	15	566 <sup>a</sup>	0.36 <sup>a</sup>	7, tw
4U 2129+47	6.3		0.63	1.4	15	374 <sup>a</sup>	0.47 <sup>a</sup>	7, 20, tw
KS 1731-26	10		1.8 <sup>a</sup>	1.4	15	524 <sup>b</sup>	0.4 <sup>a</sup>	7, tw
Neutron Stars (Z)								
Cyg X-2	100		10 <sup>a</sup>	1.9	15	346	2.2 <sup>a</sup>	8, tw
Sco X-1			7.2 <sup>a</sup>	1.4	15	310	2.3	tw, 9
GX 5-1			8.5 <sup>a</sup>	1.4	15	330	2.2	tw, 9
GX 17+2			6.9 <sup>a</sup>	1.4	15	306	2.3	tw, 9
Cir X-1	630	30	0.9 <sup>a</sup>	1.4	15	32 <sup>a</sup>	80 <sup>a</sup>	tw, 10, 11
Cir X-1	630	30	6 <sup>a</sup>	7	18	38 <sup>a</sup>	82 <sup>a</sup>	tw, 6
Black Hole Candidates								
GRS 1124-68		6.6	0.39 <sup>a</sup>	5	18.7	15 <sup>a</sup>	112 <sup>a</sup>	tw, 14, 15, 16
GS 2023+338	1008	48 <sup>a</sup>	9	7	18	39 <sup>a</sup>	95 <sup>a</sup>	tw, 18, 19, 20
1E1740.7-2942		30	< 7 <sup>a</sup>	7?	18	< 43 <sup>a</sup>	> 69 <sup>a</sup>	tw, 21
A0620-00	8		.01	4.9	18.7	13.5 <sup>a</sup>	23 <sup>a</sup>	tw, 20, 24
GRO J1655-40	31		0.25	7	18	34 <sup>a</sup>	21 <sup>a</sup>	tw, 20, 25, 26, 27
GRS 1915+105	1600	19 <sup>a</sup>	7 <sup>a</sup>	7 <sup>a</sup>	18	67 <sup>b</sup>	28 <sup>a</sup>	tw, 29, 30, 31
GS 2000+25		0.15	0.001 - 0.004 <sup>a</sup>	7	18	4.5-1.6 <sup>a</sup>	140-650 <sup>a</sup>	tw, 17, 18
Cygnus X-1		50	1 <sup>a</sup>	10	14	2.6 <sup>a</sup>	15000 <sup>a</sup>	tw, 22, 23
GRO J0422+32	?1.5		< 0.079	3.6	18	?0.23 <sup>a</sup>	?1000 <sup>a</sup>	tw, 20, 28

<sup>a</sup>Values calculated in this work.

<sup>b</sup>QPO frequency.

REFERENCES.—tw = this work, 1-Gilfanov et al. 1998, 2-Heindl & Smith 1998, 3-Campana et al 1998b, 4-Zhang, Yu & Zhang 1998, 5-Zhang et al 1998, 6-Swank 1998, 7-Campana et al 1998a, 8-Casares, Charles & Kuulkers 1998, 9-White & Zhang 1997, 10-Dower, Bradt & Morgan 1982, 11-Bradt, Shirey & Levine 1998, 12-Stella, White & Rosner 1986, 13-Cui 1997, 14-Misra & Melia 1997, 15-Ebisawa et al. 1994, 16-Życki, Done & Smith 1998, 17-Życki, Done & Smith 1997, 18- Tanaka & Lewin 1995, 19-Tanaka 1992, 20-Garcia, McClintock & Narayan 1997 21-Vilhu et al. 1997, 22-Belloni et al. 1996, 23-Misra & Melia 1997, 24-Kuulkers 1998, 25-Bailyn et al 1995, 26-Remillard et al 1997, 27-Mendez et al 1997, 28-Grove et al. 1998, 29-Belloni et al 1997, 30-Remillard et al 1997, 31-Remillard & Morgan 1998, 32-Shibata et al. 1997

TABLE 2  
QUANTITIES IN THE YILMAZ METRIC

x	f(x)	$m_b$	$m_g$	R	z	u(R)	u(0)	$gr_0/c^2$
0.150	0.993	0.001	0.001	0.148	0.009	0.009	0.013	0.061
0.250	0.980	0.006	0.006	0.242	0.023	0.023	0.033	0.098
0.350	0.961	0.015	0.014	0.328	0.044	0.043	0.063	0.138
0.450	0.936	0.030	0.028	0.406	0.071	0.069	0.102	0.182
0.550	0.907	0.053	0.047	0.474	0.105	0.100	0.149	0.234
0.650	0.873	0.085	0.072	0.531	0.145	0.136	0.203	0.293
<sup>a</sup> 0.657	0.871	0.087	0.074	0.533	0.148	0.138	0.207	0.297
0.750	0.837	0.124	0.101	0.576	0.191	0.175	0.264	0.361
0.950	0.758	0.229	0.167	0.637	0.299	0.262	0.400	0.534
1.25	0.635	0.441	0.269	0.666	0.497	0.403	0.630	0.906
1.55	0.520	0.697	0.353	0.649	0.724	0.545	0.871	1.45
1.85	0.419	0.974	0.413	0.611	0.966	0.676	1.11	2.18
2.05	0.362	1.16	0.439	0.581	1.13	0.755	1.26	2.76
2.85	0.203	1.83	0.475	0.477	1.71	0.996	1.79	5.65
3.55	0.127	2.29	0.466	0.415	2.07	1.12	2.15	8.29
4.25	0.081	2.59	0.454	0.384	2.26	1.18	2.41	10.1
7.05	0.023	3.33	0.406	0.332	2.39	1.22	3.05	12.5
10.1	0.010	3.70	0.383	0.328	2.22	1.17	3.42	11.5
15.1	0.004	4.05	0.368	0.340	1.95	1.08	3.79	9.40
20.0	0.002	4.27	0.364	0.355	1.78	1.02	4.03	8.00
40.1	0.001	4.80	0.372	0.401	1.53	0.928	4.62	5.85
60.1	0.000	5.13	0.384	0.422	1.49	0.912	4.96	5.38
80.1	0.000	5.39	0.394	0.430	1.50	0.916	5.23	5.31
100	0.000	5.60	0.401	0.434	1.52	0.924	5.44	5.39
200	0.000	6.29	0.418	0.434	1.62	0.963	6.13	5.81
400	0.000	6.98	0.425	0.434	1.67	0.982	6.83	6.04
1000.	0.000	7.90	0.431	0.434	1.70	0.993	7.74	6.17

<sup>a</sup>Entries for  $1.4 M_{\odot}$  with  $\rho_0 = 1.35 \times 10^{14} g/cm^3$ .

NOTE.—For x, f(x), see appendix. R is in units of  $r_0 = c/\sqrt{4\pi G\rho_0}$ ,  $m_b$  and  $m_g$  in units of  $M_0 = c^2 r_0/G$ . g is proper surface free-fall acceleration.

TABLE 3  
QUANTITIES IN THE SCHWARZSCHILD METRIC

x	f(x)	$m_b$	$m_g$	R	z	u(R)	u(0)	$gr_0/c^2$
0.143	0.993	0.001	0.001	0.140	0.007	0.007	0.010	0.050
0.288	0.973	0.007	0.007	0.266	0.027	0.026	0.038	0.099
0.498	0.925	0.028	0.026	0.401	0.071	0.062	0.097	0.172
0.653	0.880	0.050	0.044	0.466	0.111	0.095	0.143	0.226
0.803	0.832	0.073	0.061	0.505	0.149	0.122	0.185	0.277
0.918	0.793	0.090	0.073	0.524	0.178	0.140	0.214	0.314
<sup>a</sup> 0.923	0.792	0.091	0.074	0.525	0.180	0.141	0.215	0.316
1.003	0.765	0.102	0.081	0.534	0.199	0.152	0.234	0.341
1.153	0.716	0.122	0.093	0.545	0.231	0.170	0.264	0.385
1.353	0.655	0.143	0.104	0.550	0.269	0.190	0.297	0.438
1.513	0.609	0.157	0.111	0.550	0.295	0.202	0.318	0.475
1.653	0.573	0.168	0.115	0.549	0.314	0.210	0.334	0.503
1.853	0.526	0.180	0.120	0.546	0.336	0.220	0.353	0.539
2.053	0.484	0.190	0.123	0.542	0.354	0.227	0.368	0.569
2.353	0.430	0.201	0.126	0.536	0.375	0.236	0.386	0.604
2.753	0.373	0.211	0.128	0.529	0.393	0.242	0.404	0.639
3.053	0.338	0.216	0.129	0.524	0.403	0.246	0.414	0.658
3.553	0.291	0.222	0.129	0.518	0.413	0.250	0.427	0.680
4.053	0.255	0.226	0.129	0.514	0.419	0.252	0.437	0.695
4.998	0.206	0.231	0.129	0.508	0.424	0.253	0.449	0.710
6.050	0.168	0.233	0.129	0.504	0.429	0.255	0.458	0.725
8.050	0.125	0.235	0.128	0.501	0.427	0.254	0.469	0.725
10.05	0.100	0.235	0.127	0.500	0.425	0.254	0.475	0.722
15.05	0.066	0.236	0.126	0.500	0.421	0.252	0.483	0.717
20.00	0.050	0.236	0.126	0.500	0.419	0.252	0.488	0.713

<sup>a</sup>Entries for  $1.4 M_{\odot}$  with  $\rho_0 = 1.35 \times 10^{14} g/cm^3$ .

NOTE.—For x, f(x), see appendix. R is in units of  $r_0 = c/\sqrt{4\pi G\rho_0}$ ,  $m_b$  and  $m_g$  in units of  $M_0 = c^2 r_0/G$ . g is proper surface free-fall acceleration.